Inorganic Chemistry
Article

Inorg. Chem. **2010**, *49*, 7497–7509 **7497**
DOI: 10.1021/ic101012a

Long-Range Electronic Communication in Free-Base *meso*-Poly(Ferrocenyl)-Containing Porphyrins

Victor N. Nemykin,*,† Gregory T. Rohde,† Christopher D. Barrett,† Ryan G. Hadt,† Jared R. Sabin,† Giacomo Reina,†,‡ Pierluca Galloni,*,‡ and Barbara Floris‡

†*Department of Chemistry & Biochemistry, University of Minnesota Duluth, Duluth, Minnesota 55812, and* ‡*Dipartimento di Scienze e Tecnologie Chimiche, Università di Roma "Tor Vergata", via della ricerca scientifica, 00133 Rome, Italy*

Received May 19, 2010

H_2FcPh_3P [$FcPh_3P$ = 5-ferrocenyl-10,15,20-triphenyl porphyrin(2-)], *cis*-$H_2Fc_2Ph_2P$ [*cis*-Fc_2Ph_2P = 5,10-bisferrocenyl-15,20-diphenyl porphyrin(2-)], *trans*-$H_2Fc_2Ph_2P$ [*trans*-Fc_2Ph_2P = 5,15-bisferrocenyl-10,20-diphenyl porphyrin(2-)], and H_2Fc_3PhP [Fc_3PhP = 5,10,15-trisferrocenyl-20-phenyl porphyrin(2-)] along with H_2TPP [TPP = 5,10,15,20-tetraphenylporphyrin] and H_2TFcP [TFcP = 5,10,15,20-tetraferrocenyl porphyrin(2-)] were isolated from the direct cross-condensation reaction between pyrrole, benzaldehyde, and ferrocene carboxaldehyde or from the reaction between ferrocenyl-2,2′-dipyrromethane and benzaldehyde, suggesting a scrambling reaction mechanism for the last approach. All compounds were characterized by UV−vis, MCD, and NMR spectroscopy; APCI MS and MS/MS methods; as well as high-resolution ESI MS spectrometry. The conformational flexibility of ferrocene substituents in all compounds was confirmed using variable-temperature NMR and computational methods. DFT calculations were employed to understand the degree of nonplanarity of the porphyrin core as well as the electronic structure of ferrocene-containing porphyrins. In all cases, a set of occupied, predominantly ferrocene-based molecular orbitals was found between the highest occupied and the lowest unoccupied, predominantly porphyrin-based molecular π orbitals. The redox properties of all ferrocene-containing porphyrins were investigated in a CH_2Cl_2/TFAB [TFAB = tetrabutylammonium tetrakis(perfluorophenyl)borate] system using cyclic voltammetry, differential pulse voltammetry, and square wave voltammetry methods. In all cases, oxidations of individual ferrocene substituent(s) along with porphyrin core oxidation(s) and reductions have been observed. Mixed-valence [*cis*-$H_2Fc_2Ph_2P]^+$, [*trans*-$H_2Fc_2Ph_2P]^+$, $[H_2Fc_3PhP]^+$, and $[H_2Fc_3PhP]^{2+}$ complexes were formed *in situ* under spectroelectrochemical and chemical oxidation conditions and were characterized using UV−vis and MCD approaches. Analysis of intervalence charge-transfer bands observed in the NIR region for all mixed-valence complexes suggests electron localization and thus class II behavior in the Robin−Day classification.

Introduction

Ferrocenyl-containing porphyrins,[1−3] tetraazaporphyrins,[4] phthalocyanines,[5] corroles,[6] and their nonaromatic analogues[7] represent a relatively new and exciting class of macrocyclic compounds. These macrocycles have been studied because of their potentially interesting multiple ferrocene- and macrocycle-based redox processes, long-range metal−metal coupling, photoinduced electron transfer processes, and unpaired electron density migration.[1a,8] In addition, these nanomeric-sized multinuclear switchable arrays are also interesting from a practical point of view. For instance, molecular-based electronic devices such as molecular multibit information storage elements, molecular electrogenic sensors, and molecular modules that mimic photosynthetic active sites can find widespread use in modern society.[9] In many of these applications, formation of the mixed-valence (MV) states in ferrocene-containing macrocycles is responsible for the above-mentioned properties. Factors affecting the formation and stability of the MV states in multinuclear ferrocene derivatives have been thoroughly investigated.[10] In most cases, effective metal−metal coupling between ferrocene units in the same molecule can be achieved when Fe−Fe distances are shorter than 5−6 Å, while examples of long-range (> 10 Å) metal−metal coupling in polyferrocenyl-containing systems are still rare.[1c,e,h,l,o,q]

One of the most interesting examples of strong, long-range (> 10 Å) metal−metal coupling was presented by Burrell et al. in 1999 for the metal-free and nickel α,α-5,15-bis(ferrocenyl)-2,8,12,18-tetrabutyl-3,7,13,17-tetramethylporphyrins[1c] and was further confirmed by another research group for the metal-free and manganese α,α-5,15-bis(ferrocenyl)-2,8,12,18-tetrabutyl-3,7,13,17-tetraethylporphyrins.[1e] In both cases, pure atropisomers of the metal-free and transition-metal α,α-5,15-bis(ferrocenyl)-2,3,7,8,12,13,17,18-octaalkylporphyrins demonstrated long-range metal−metal coupling between two

*To whom correspondence should be addressed. E-mail: vnemykin@d.umn.edu (V.N.N.), galloni@scienze.uniroma2.it (P.G.).

Published on Web 07/20/2010

ferrocenyl substituents due to restricted conformational flexibility of the ferrocene groups. In accordance with this hypothesis, other *meso*-tetraferrocenyl porphyrin systems, with the ferrocenyl units connected to the porphyrin core through aromatic linking groups, were reported to be unable to form MV complexes.[2] It was shown recently, however, that electrochemical oxidation of the metal-free 5,10,15,20-tetraferrocenylporphyrin (H_2TFcP) in a noncoordinating solvent in the presence of a noncoordinating electrolyte as well as its chemical oxidations by a variety of the oxidants results in the formation of several MV complexes, which were characterized by UV−vis−NIR, MCD, IR, Mössbauer, and XPS spectroscopy.[1r] One of the interesting issues, which originated from the electrochemical and chemical oxidation data of H_2TFcP, was the nature of the MV $[H_2TFcP]^{2+}$ complex. Indeed, the removal of an electron from $[H_2TFcP]^{+}$ can result in the formation of $[H_2(5,10\text{-}Fc^{+}{}_2)(15,20\text{-}Fc_2)P]^{2+}$ (adjacent isomer) or $[H_2(5,15\text{-}Fc^{+}{}_2)(10,20\text{-}Fc_2)P]^{2+}$ (opposite isomer) complexes.

In order to understand how the ferrocene substituents located at specific *meso* positions in polyferrocenyl-containing porphyrins can influence long-range metal−metal coupling, we prepared, characterized, and investigated redox properties of H_2FcPh_3P [$FcPh_3P$ = 5-ferrocenyl-10,15,20-triphenyl porphyrin(2-)], *cis*-$H_2Fc_2Ph_2P$ [*cis*-Fc_2Ph_2P = 5,10-bisferrocenyl-15,20-diphenyl porphyrin(2-)], *trans*-$H_2Fc_2Ph_2P$ [*trans*-Fc_2Ph_2P = 5,15-bisferrocenyl-10,20-diphenyl porphyrin(2-)], and H_2Fc_3PhP [Fc_3PhP = 5,10,15-trisferrocenyl-20-phenyl porphyrin(2-)] compounds (Scheme 1). A specific question addressed below is whether or not the extended π system of the porphyrin core is a good platform for electron transfer processes between ferrocene substituents located at *meso* positions.

Experimental Section

Materials. All reactions were performed under a dry argon atmosphere with flame-dried glassware. Pyrrole, ferrocenecarbaldehyde, benzaldehyde, $BF_3\cdot Et_2O$, chloranil, DDQ, ferrocene, decamethylferrocene, silver triflate, nitrosonium tetrafluoroborate, and triethylamine were purchased from commercially available sources and used without further purification. Silica gel (60 Å, 32−63 mesh) was purchased from Sorbent Technologies. Basic aluminum oxide (Activity I, 58 Å, 150 mesh) was purchased from Fischer Inc. Bio-Beads (SX-1 and SX-3) for size exclusion filtration were purchased from Bio-Rad. All solvents were dried with appropriate drying agents (molecular sieves for $CHCl_3$; CaH_2 for toluene, DCM, and *o*-DCB; sodium for THF and diethyl ether) and distilled directly prior to experiments. Tetrabutylammonium tetrakis(perfluorophenyl)borate (TFAB) was prepared according to the

(1) (a) Bucher, C.; Devillers, C. H.; Moutet, J.-C.; Royal, G.; Saint-Aman, E. *Coord. Chem. Rev.* **2009**, *253*, 21–36. (b) Loim, N. M.; Abramova, N. V.; Sokolov, V. I. *Mendeleev Commun.* **1996**, 46–47. (c) Burrell, A. K.; Campbell, W. M.; Jameson, G. B.; Officer, D. L.; Boyd, P. D. W.; Zhao, Z.; Cocks, P. A.; Gordon, K. C. *Chem. Commun.* **1999**, 637–638. (d) Narayanan, S. J.; Venkatraman, S.; Dey, S. R.; Sridevi, B.; Anand, V. R. G.; Chandrashekar, T. K. *Synlett* **2000**, 1834–1836. (e) Rhee, S. W.; Na, Y. H.; Do, Y.; Kim, J. *Inorg. Chim. Acta* **2000**, *309*, 49–56. (f) Rhee, S. W.; Park, B. B.; Do, Y.; Kim, J. *Polyhedron* **2000**, *19*, 1961–1966. (g) Kim, J.; Rhee, S. W.; Na, Y. H.; Lee, K. P.; Do, Y.; Jeoung, S. C. *Bull. Korean Chem. Soc.* **2001**, *22*, 1316–1322. (h) Nemykin, V. N.; McGinn, M.; Koposov, A. Y.; Tretyakova, I. N.; Polshin, E. V.; Loim, N. M.; Abramova, N. V. *Ukr. Khim. Zh.* (*Russ. Ed.*) **2005**, *71*, 79–85. (i) Shoji, O.; Okada, S.; Satake, A.; Kobuke, Y. *J. Am. Chem. Soc.* **2005**, *127*, 2201–2210. (j) Shoji, O.; Tanaka, H.; Kawai, T.; Kobuke, Y. *J. Am. Chem. Soc.* **2005**, *127*, 8598–8599. (k) Niemevz, F.; Martinez, J. M. L.; Carballo, R.; Rezzano, I.; Buldain, G. Y. *Synthesis* **2006**, 870–874. (l) Auger, A.; Swarts, J. C. *Organometallics* **2007**, *26*, 102–109. (m) Kubo, M.; Mori, Y.; Otani, M.; Murakami, M.; Ishibashi, Y.; Yasuda, M.; Hosomizu, K.; Miyasaka, H.; Imahori, H.; Nakashima, S. *J. Phys. Chem. A* **2007**, *111*, 5136–5143. (n) Morisue, M.; Kalita, D.; Haruta, N.; Kobuke, Y. *Chem. Commun.* **2007**, 2348–2350. (o) Nemykin, V. N.; Barrett, C. D.; Hadt, R. G.; Subbotin, R. I.; Maximov, A. Y.; Polshin, E. V.; Koposov, A. Y. *Dalton Trans.* **2007**, 3378–3389. (p) Rochford, J.; Rooney, A. D.; Pryce, M. T. *Inorg. Chem.* **2007**, *46*, 7247–7249. (q) Nemykin, V. N.; Galloni, P.; Floris, B.; Barrett, C. D.; Hadt, R. G.; Subbotin, R. I.; Marrani, A. G.; Zanoni, R.; Loim, N. M. *Dalton Trans.* **2008**, 4233–4246. (r) Nemykin, V. N.; Rohde, G. T.; Barrett, C. D.; Hadt, R. G.; Bizzarri, C.; Galloni, P.; Floris, B.; Nowik, I.; Herber, R. H.; Marrani, A. G.; Zanoni, R.; Loim, N. M. *J. Am. Chem. Soc.* **2009**, *131*, 14969–14978. (s) Gryko, D. T.; Zhao, F.; Yasseri, A. A.; Roth, K. M.; Bocian, D. F.; Kuhr, W. G.; Lindsey, J. S. *J. Org. Chem.* **2000**, *65*, 7356–7362. (t) Galloni, P.; Floris, B.; de Cola, L.; Cecchetto, E.; Williams, R. M. *J. Phys. Chem. C* **2007**, *111*, 1517–1523.

(2) (a) Burrell, A. K.; Campbell, W.; Officer, D. L. *Tetr. Lett.* **1997**, *38*, 1249. (b) Burrell, A. K.; Campbell, W. M.; Officer, D. L.; Scott, S. M.; Gordon, K. C.; McDonald, M. R. *J. Chem. Soc., Dalton Trans.* **1999**, 3349. (c) Jiao, L.; Courtney, B. H.; Fronczek, F. R.; Smith, K. M. *Tetr. Lett.* **2006**, *47*, 501. (d) Wang, H. J. H.; Jaquinod, L.; Nurco, D. J.; Vicente, M. G. H.; Smith, K. M. *Chem. Commun.* **2001**, 2646. (e) Wang, H. J. H.; Jaquinod, L.; Olmstead, M. M.; Vicente, M. G. H.; Kadish, K. M.; Ou, Z.; Smith, K. M. *Inorg. Chem.* **2007**, *46*, 2898.

(3) (a) Gryko, D. T.; Zhao, F.; Yasseri, A. A.; Roth, K. M.; Bocian, D. F.; Kuhr, W. G.; Lindsey, J. S. *J. Org. Chem.* **2000**, *65*, 7356. (b) Schmidt, E. S.; Calderwood, T. S.; Bruice, T. C. *Inorg. Chem.* **1986**, *25*, 3718. (c) Cheng, K.-L.; Li, H.-W.; Ng, D. K. P. *J. Organomet. Chem.* **2004**, *689*, 1593. (d) Giasson, R.; Lee, E. J.; Zbao, X.; Wrighton, M. S. *J. Phys. Chem.* **1993**, *97*, 2596. (e) Cammidge, A. N.; Scaife, P. J.; Berber, G.; David, L. H. *Org. Lett.* **2005**, *7*, 3413. (f) Muraoka, T.; Kinbara, K.; Aida, T. *Nature* **2006**, *440*, 512. (g) Maiya, G. B.; Barbe, J. M.; Kadish, K. M. *Inorg. Chem.* **1989**, *28*, 2524–2527.

(4) (a) Nemykin, V. N.; Kobayashi, N. *Chem. Commun.* **2001**, 165–166. (b) Lukyanets, E. A.; Nemykin, V. N. *J. Porphyrins Phthalocyanines* **2010**, *14*, 1–40.

(5) (a) Jin, Z.; Nolan, K.; McArthur, C. R.; Lever, A. B. P.; Leznoff, C. C. *J. Organomet. Chem.* **1994**, *468*, 205–12. (b) Poon, K.-W.; Yan, Y.; Li, X. Y.; Ng, D. K. P. *Organometallics* **1999**, *18*, 3528. (c) Salan, U.; Altindal, A.; Bulut, M.; Bekaroglu, O. *J. Porphyrins Phthalocyanines* **2006**, *10*, 1263–1270. (d) McKeown, N. B. In *The Porphyrin Handbook*; Academic Press: New York, 2003; Vol. *15*, pp 61−124. (e) Nemykin, V. N.; Lukyanets, E. A. In *Handbook of Porphyrin Science*; Kadish, K. K., Smith, K. M., Guilard, R., Eds.; World Scientific: Singapore, 2010; Vol. *3*, pp 1−323. (f) Nemykin, V. N.; Lukyanets, E. A. *ARKIVOC* **2010**, (i), 136–208.

(6) (a) Gryko, D. T.; Piechowska, J.; Jaworski, J. S.; Galezowski, M.; Tasior, M.; Cembor, M.; Butenschoen, H. *New J. Chem.* **2007**, *31*, 1613–1619. (b) Kumar, R.; Misra, R.; PrabhuRaja, V.; Chandrashekar, T. K. *Chem.—Eur. J.* **2005**, *11*, 5695–5707. (c) Venkatraman, S.; Kumar, R.; Sankar, J.; Chandrashekar, T. K.; Sendhil, K.; Vijayan, C.; Kelling, A.; Senge, M. O. *Chem.—Eur. J.* **2004**, *10*, 1423–1432.

(7) (a) Bucher, C.; Devillers, C. H.; Moutet, J.-C.; Pecaut, J.; Royal, G.; Saint-Aman, E.; Thomas, F. *Dalton Trans.* **2005**, 3620–3631. (b) Szymanska, I.; Radecka, H.; Radecki, J.; Gale, P. A.; Warriner, C. N. *J. Electroanal. Chem.* **2006**, *591*, 223–228. (c) Gale, P. A.; Hursthouse, M. B.; Light, M. E.; Sessler, J. L.; Warriner, C. N.; Zimmerman, R. S. *Tetrahedron Lett.* **2001**, *42*, 6759–6762.

(8) (a) Grimm, B.; Hausmann, A.; Kahnt, A.; Seitz, W.; Spanig, F.; Guldi, D. M. In *Handbook of Poprhyrin Science*; Kadish, K. K., Smith, K. M., Guilard, R., Eds.; World Scientific: Singapore, 2010; Vol. *1*, pp 133 − 219. (b) Suijkerbuijk, B. M. J. M.; Gebbink, R. J. M. K. *Angew. Chem., Int. Ed.* **2008**, *47*, 7396–7421.

(9) (a) Miller, J. S.; Epstein, A. J. *Angew. Chem., Int. Ed.* **1994**, *33*, 385. (b) Epstein, A. J.; Miller, J. S. *Synth. Met.* **1996**, *80*, 231. (c) Barlow, S. *Inorg. Chem.* **2001**, *40*, 7047. (d) Barlow, S.; O'Hare, D. *Chem. Rev.* **1997**, *97*, 637. (e) Kaim, W.; Lahiri, G. K. *Angew. Chem., Int. Ed.* **2007**, *46*, 1778–1796. (f) Kaim, W.; Sarkar, B. *Coord. Chem. Rev.* **2007**, *251*, 584–594. (g) Chisholm, M. H.; Patmore, N. J. *Acc. Chem. Res.* **2007**, *40*, 19–27. (h) Solomon, E. I.; Sarangi, R.; Woertink, J. S.; Augustine, A. J.; Yoon, J.; Ghosh, S. *Acc. Chem. Res.* **2007**, *40*, 581–591.

(10) (a) Cowan, D. O.; Kaufman, F. *J. Am. Chem. Soc.* **1970**, *92*, 6198. (b) Cowan, D. O.; Kaufman, F. *J. Am. Chem. Soc.* **1970**, *92*, 219. (c) Morrison, W. H., Jr.; Hendrickson, D. N. *Chem. Phys. Lett.* **1973**, *22*, 119. (d) Morrison, W. H., Jr.; Krogsrud, S.; Hendrickson, D. N. *Inorg. Chem.* **1973**, *12*, 1998. (e) Morrison, W. H., Jr.; Hendrickson, D. N. *Inorg. Chem.* **1975**, *14*, 2331. (f) Dong, T. Y.; Hendrickson, D. N. *Bull. Inst. Chem., Acad. Sinica* **1987**, *34*, 67. (g) Tolbert, L. M.; Zhao, X.; Ding, Y.; Bottomley, L. A. *J. Am. Chem. Soc.* **1995**, *117*, 12891. (h) Ribou, A.-C.; Launay, J.-P.; Sachtleben, M. L.; Li, H.; Spangler, C. W. *Inorg. Chem.* **1996**, *35*, 3735. (i) Patoux, C.; Coudret, C.; Launay, J.-P.; Joachim, C.; Gourdon, A. *Inorg. Chem.* **1997**, *36*, 5037. (j) Hadt, R. G.; Nemykin, V. N. *Inorg. Chem.* **2009**, *48*, 3982.

Scheme 1. Synthetic Pathway for Preparation of the Target Ferrocenyl-Containing Porphyrins

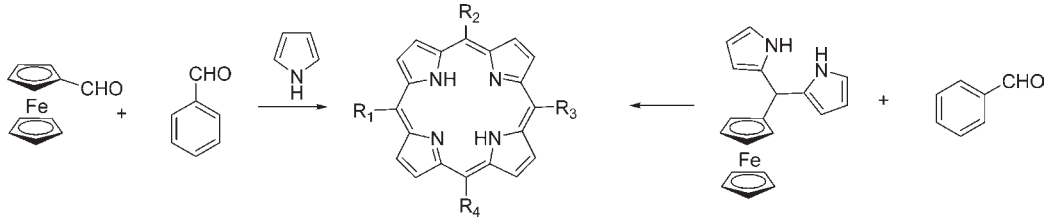

H_2TPP: R_1 - R_4 = Ph
H_2FcPh_3P: R_1 = Fc; R_2 - R_4 = Ph
cis-$H_2Fc_2Ph_2P$: R_1 = R_2 = Fc; R_3 = R_4 = Ph
trans-$H_2Fc_2Ph_2P$: R_1 = R_3 = Fc; R_2 = R_4 = Ph
H_2Fc_3PhP: R_1 - R_3 = Fc; R_4 = Ph
H_2TFcP: R_1 - R_4 = Fc

literature,[11] by a metathesis reaction between lithium tetrakis-(perfluorophenyl)borate and tetrabutylammonium bromide.

Physical Measurements. UV−vis−NIR data were obtained on Jacso V-670 or Cary 17 spectrometers. MCD data were recorded using an OLIS DCM 17 CD spectropolarimeter using a permanent 1.4 T DeSa magnet. The spectra were recorded twice for each sample, once with a parallel field and again with an antiparallel field, and their intensities were expressed by molar ellipticity per $T = [\Theta]_M$/deg dm^3 mol^{-1} cm^{-1} T^{-1}. Electrochemical measurements were conducted using a CH electrochemical analyzer utilizing a three-electrode scheme with platinum or glassy carbon working electrodes and platinum wires as auxiliary and pseudo reference electrodes. Dry degassed dichloromethane and a 0.05 M solution of the TFAB electrolyte were used in all electrochemical experiments. Potentials were corrected using the internal standard (decamethylferrocene, $Me_{10}Fc$) in all cases. Potentials were then corrected to ferrocene using appropriate oxidation potentials for $Me_{10}Fc/Me_{10}Fc^+$ vs Fc/Fc^+ in the DCM/TFAB system.[11] Spectroelectrochemical data were collected in a 0.15 M solution of TFAB in DCM at the appropriate oxidation potentials using a custom-made spectroelectrochemical cell. Oxidation reversibility experiments were conducted at −0.3 V potentials. NMR spectra were recorded on a Varian INOVA instrument with a 500 MHz frequency for protons and 125 MHz for carbon. Chemical shifts are reported in parts per million and referenced to TMS as an internal standard. In all cases, final assignments of ^{1}H and ^{13}C signals were made using COSY and HMQC spectra. APCI-MS and APCI-MS/MS experiments were conducted in THF using a Finnegan LCQ LC-MS system. High-resolution mass spectra were obtained in THF/MeOH using a Bruker Daltonics HRMS instrument.

X-Ray Crystallography. Single crystals of H_2TFcP (0.04 × 0.14 × 0.16 mm) suitable for X-ray crystallographic analysis were obtained by the slow evaporation of a dichloromethane/hexane (5:1 v/v) solution of H_2TFcP. X-ray diffraction data were collected on a Rigaku RAPID II diffractometer using a graphite monochromator and Mo Kα radiation (λ = 0.71073 Å) at −173 °C. Multiscan absorption correction was applied to the data using the HKL2000 program.[12] Four twin components were indexed using CrystalClear 2.0 software[13] (R_{int} = 12.3%). The crystal structure was solved on the best twin component data by direct methods (SIR-92)[14] and refined by full-matrix least-squares refinement on F^2 using the Crystals for Windows program.[15] Crystal data for $C_{60}H_{46}Fe_4N_4$: M = 1046.44, tetragonal, space group $P\bar{4}21/c$, a = 12.2883(5), b = 12.2883(5), c = 14.8822(6) Å, V = 2247.23(16) Å^3, Z = 2 (asymmetric unit cell comprises 1/4 of a porphyrin ring), μ = 1.313 mm^{-1}, 49 479 reflections measured, 3295 unique. final R_1 = 0.0340, R_w = 0.0857. CCDC 773704 contains the supplementary crystallographic data for H_2TFcP. These data can be obtained free of charge via www.ccdc.cam.ac.uk/conts/retrieving.html (or from Cambridge Crystallographic Data Centre, 12 Union Road, Cambridge CB2 1EZ U. K.; fax: (+44) 1223-336-033 or deposit@ccdc.cam.ac.uk).

Computational Aspects. All DFT calculations were conducted using the *Gaussian 03* software package running under either a Windows or UNIX OS.[16] The molecular geometries were obtained via optimization with Becke's exchange functional[17] and the Perdew nonlocal correlation functional (BPW91)[18] coupled with Wachter's full-electron basis set for the iron[19] atom and the 6-31G(d) basis set[20] for all other atoms. For all optimized structures, frequency calculations were carried out to ensure that optimized geometries represented local minima. When necessary, the percent contributions of atomic orbitals to molecular orbitals were calculated using the VMOdes program.[21]

Synthesis of Ferrocenyl-Containing Porphyrins. Statistical Condensation Approach. A mixture of 0.60 g (0.0028 mol) of ferrocenecarbaldehyde, 0.30 g (0.0028 mol) of benzaldehyde, 0.40 g (0.0060 mol) of pyrrole, and 0.038 mL (0.0003 mol) of $BF_3 \cdot Et_2O$ in CH_2Cl_2 (150 mL) was reacted for 20 h at room temperature in an argon atmosphere. After this period, 0.98 g (0.0040 mol) of chloranil was added, and the resulting mixture was refluxed for an additional 3.5 h. After solvent evaporation, the residue was chromatographed first on activity I alumina to eliminate the majority of the linear oligomeric reaction byproduct. After this step, individual asymmetric porphyrins were separated using several sets of preparative silica gel TLC plates using a toluene−hexane−triethylamine mixture (69:29:2 v/v) as an eluent. Individual fractions were collected and further purified using size-exclusion SX-1 and SX-3 columns, and finally, target porphyrins were recrystallized from a toluene−hexane mixture.

Yields of isolated products and analytic data for target compounds (see Supporting Information Figure 1 for ^{1}H NMR

(11) (a) Barriere, F.; Geiger, W. E. *J. Am. Chem. Soc.* **2006**, *128*, 3980. (b) Geiger, W. E.; Connelly, N. G. *Adv. Organomet. Chem.* **1985**, *24*, 87.
(12) Otwinowski, Z.; Minor, W. In *Methods in Enzymololgy*; Carter, C. W., Jr., Sweet, R. M., Eds.; Academic Press: New York, 1997; Vol. *276* Macromolecular Crystallography, part A, pp 307−326.
(13) *Crystal Clear SM*, version 2.0; Rigaku Americas Corporation: The Woodlands, TX, 1998−2009.
(14) Altomare, A.; Cascarano, G.; Giacovazzo, G.; Guagliardi, A.; Burla, M. C.; Polidori, G.; Camalli, M. *J. Appl. Crystallogr.* **1994**, *27*, 435.
(15) Betteridge, P. W.; Carruthers, J. R.; Cooper, R. I.; Prout, K.; Watkin, D. J. *J. Appl. Crystallogr.* **2003**, *36*, 1487.
(16) Frisch, M. J. et al. *GAUSSIAN 03*, revision C.02; Gaussian, Inc.: Wallingford, CT, 2004. See the Supporting Information for a full citation.
(17) Becke, A. D. *Phys. Rev. A* **1988**, *38*, 3098.
(18) Lee, C.; Yang, W.; Parr, R. G. *Phys. Rev. B* **1988**, *37*, 785.
(19) Wachters, A. J. H. *J. Chem. Phys.* **1970**, *52*, 1033.
(20) McLean, A. D.; Chandler, G. S. *J. Chem. Phys.* **1980**, *72*, 5639.
(21) Nemykin, V. N.; Basu, P. *VMOdes: Virtual Molecular Orbital description program for Gaussian, GAMESS, and HyperChem*, Revision A 7.2; Univeristy of Minnesota, Duluth, MN, 2003.

spectra and Supporting Information Figure 2 for APCI MS and ESI HRMS spectra; when necessary, ^{1}H and ^{13}C NMR peaks were assigned on the basis of COSY and HMQC spectra).

H_2TPP. Yield: 31 mg (3.6%). Selected spectroscopic data are identical to the commercially available sample. UV−vis (λ_{max}/nm, $CHCl_3$, log ε): 417 (5.50), 512 (4.11), 550 (3.59), 590 (3.57), 647 (3.55). ^{1}H NMR ($CDCl_3$, TMS, δ): 8.84 (s, 8H, β-pyrr), 8.20−8.23 (m, 8H, *o*-Ph), 7.73−7.75 (m, 12H, *m*+*p*-Ph), −2.76 (s, 2H, NH). MS (APCI, THF, *m*/*z*): 615 (100%) $[M + H]^+$.

H_2FcPh$_3$P. Yield: 96 mg (9.5%). Selected spectroscopic data, UV−vis (λ_{max}/nm, $CHCl_3$, log ε): 421 (5.50), 511 (4.04), 602 (3.88), 672 (3.86). ^{1}H NMR ($CDCl_3$, TMS, δ): 9.98 (d, J = 4 Hz, 2H, β-pyrr-Ph-**Fc**), 8.73−8.78 (m, 6H, β-pyrr-Ph-Fc), 8.17−8.21 (m, 6H, *o*-Ph), 7.72−7.78 (m, 9H, *m*+*p*-Ph), 5.54 (t, *J* = 2 Hz, 2H, α-Cp), 4.82 (t, *J* = 2 Hz, 2H, β-Cp), 4.16 (s, 5H, CpH), −2.29 (s, 2H, NH). ^{13}C NMR ($CDCl_3$, TMS, δ): 146 (α-pyrr, vbr), 142.6 (C_i-$Ph_{1,3}$), 142.0 (C_i-Ph_2), 131.4 (β-pyrr-Ph-Fc, vbr), 130.6 (β-pyrr, vbr), 134.7 (*o*-Ph), 127.9 (*m*+*p* −Ph), 127.0 (*m*+*p* −Ph), 126.9 (*m*+*p* −Ph), 120.4 (*meso*-C-$Ph_{1,3}$), 119.9 (*meso*-C-Ph_2), 118.5 (*meso*-C-Cp), 89.7 (C_i-Cp), 77.7 (α-Cp), 70.9 (CpH), 69.3 (β-Cp). MS (APCI, THF, *m*/*z*): 723.19 (100%) $[M + H]^+$. HRMS (ESI, THF/MeOH, *m*/*z*): 723.2208 (calcd for $C_{48}H_{35}N_4Fe$: 723.2207).

***trans*-$H_2Fc_2Ph_2P$.** Yield: 6 mg (0.5%). Selected spectroscopic data, UV−vis (λ_{max}/nm, $CHCl_3$, log ε): 426 (5.19), 500sh, 633 (3.88), 705 (3.92). ^{1}H NMR ($CDCl_3$, TMS, δ): 9.82 (d, *J* = 4.5 Hz, 4H, β-pyrr-Fc); 8.66 (d, *J* = 4.5 Hz, β-pyrr-Ph); 8.18 (dd, *J* = 8 Hz, 1.5 Hz, 4H, *o*-Ph); 7.72−7.77 (m, 6H, *m*+*p* -Ph); 5.50 (t, *J* = 1.5 Hz, 4H, α-Cp); 4.81 (t, *J* = 1.5 Hz, 4H, β-Cp); 4.12 (s, 10H, CpH); −1.66 (s, 2H, NH). MS (APCI, THF, *m*/*z*): 831.24 (100%) $[M + H]^+$. HRMS (ESI, THF/MeOH, *m*/*z*): 831.1848 (calcd for $C_{52}H_{39}N_4Fe_2$: 831.1871).

***cis*-$H_2Fc_2Ph_2P$.** Yield: 14 mg (1.2%). Selected spectroscopic data, UV−vis (λ_{max}/nm, $CHCl_3$, log ε): 423 (5.15), 515 (3.94), 598 (3.90), 695 (3.81). ^{1}H NMR ($CDCl_3$, TMS, δ): 9.90 (s, 2H, β-pyrr-Cp-Cp), 9.78 (d, *J* = 5 Hz, 2H, β-pyrr-Ph-Cp), 8.71 (d, *J* = 5 Hz, 2H, β-pyrr-Ph-Cp), 8.65 (s, 2H, β-pyrr-Ph-Ph), 8.15 (d, *J* = 6 Hz, 4H, α-Ph), 7.72 (t, *J* = 6 Hz, 6H, β-Ph + γ-Ph), 5.45 (s, 4H, α-*Pc*), 4.76 (s, 4H, β-Cp), 4.06 (s, 10H, CpH), −1.83 (s, 2H, NH). ^{13}C NMR ($CDCl_3$, TMS, δ), 156.7 (α-pyrr-Cp-Cp, vbr), 143.9 (β-pyrr-Ph-Ph, vbr), 141.0 (C_i-Ph), 133.4 ($C_{2,6}$-Ph), 130.2 (β-pyrr-Cp-Cp), 129.6 (β-pyrr-Cp-Ph), 129.5 (β-pyrr-Cp-Ph), 128.9 (β-pyrr-Ph-Ph), 126.6 (C_4−Ph), 125.7 ($C_{3,5}$-Ph), 118.7 (*meso*-C-Cp), 117.1 (*meso*-C-Ph), 88.6 (C_i-Cp), 76.5 (α-Cp), 69.5 (CpH), 68.0 (β-Cp). MS (APCI, THF, *m*/*z*): 831.25 (100%) [M + H]. HRMS (ESI, THF, *m*/*z*): 831.1867 (calcd for $C_{52}H_{39}N_4Fe_2$: 831.1871).

H_2Fc_3PhP. Yield: 34 mg (2.6%). Selected spectroscopic data, UV−vis (λ_{max}/nm, $CHCl_3$, log ε): 429 (5.19), 495sh, 641 (4.06), 713 (4.03). ^{1}H NMR ($CDCl_3$, TMS, δ): 9.74 − 9.77 (m, 4H, β-pyrr-Fc-Fc); 6.66 (d, *J* = 5 Hz, 2H, β-pyrr-Fc-Ph); 8.58 (d, *J* = 5 Hz, 2H, β-pyrr-Fc-Ph); 8.13 (dd, *J* = 7.5 Hz, 1.5 Hz, 2H, *o*-Ph); 7.70−7.77 (m, 3H, *m*+*p* Ph); 5.43 (t, *J* = 2 Hz, 4H, α-$Cp_{1,3}$); 5.41 (t, *J* = 2 Hz, 2H, α-Cp_2); 4.81 (t, *J* = 2 Hz, 2H, β-Cp_2); 4.79 (t, *J* = 2 Hz, 4H, β-$Cp_{1,3}$); 4.05 (s, 10H, $CpH_{1,3}$); 4.04 (s, 5H, CpH_2); −1.13 (s, 2H, NH). ^{13}C NMR ($CDCl_3$, TMS, δ): 146.0 (α-pyrr, vbr), 134.6 (*o*-Ph), 132.7 (*i*-Ph), 131.5 (β-pyrr-Fc-Ph), 131.2 (β-pyrr-Fc-Fc), 130.7 (β-pyrr-Fc-Fc), 130.4 (β-pyrr-Fc-Ph), 129.1 (*m*-Ph), 127.0, (*p*-Ph), 118.9 (*meso*-C-Ph), 117.0 (*meso*-C-Cp_2), 116.7 (*meso*-C-$Cp_{1,3}$), 89.4 (C_i-Cp), 77.2 (α-$Cp_{1,2,3}$), 70.7 ($CpH_{1,3}$), 70.6 (CpH_2), 68.4 (β-$Cp_{1,3}$), 68.3 (β-Cp_2). MS (APCI, THF, *m*/*z*): 939.11 (100%) $[M + H]^+$. HRMS (ESI, THF/MeOH, *m*/*z*): 939.1472 (calcd for $C_{56}H_{43}N_4Fe_3$: 939.1535).

H_2TFcP. Yield: 28 mg (1.9%). Spectroscopic data are identical to the earlier reported[1q] samples. UV−vis (λ_{max}/nm, $CHCl_3$, log ε): 434 (5.08), 485sh, 661 (4.24), 726 (4.18). ^{1}H NMR ($CDCl_3$, TMS, δ): 9.61 (s, 8H, β-pyrr); 5.32 (t, 8H, α-Cp); 4.75 (t, 8H, β-Cp); 3.97 (s, 20H, CpH); −0.49 (s, 2H, NH). ^{13}C NMR ($CDCl_3$, TMS, δ): 145.8 (α-pyrr, vbr); 130.6 (β-pyrr); 117.1 (C_{meso}); 88.9 (Cp_{ipso}); 76.6 (α-Cp); 70.1 (CpH); 68.8 (β-Cp). MS (APCI, THF, *m*/*z*): 1047.13 (100%) $[M + H]^+$. HRMS (ESI, THF/MeOH, *m*/*z*): 1047.1193 (1047.1200 calcd for $C_{60}H_{47}N_4Fe_4$).

Condensation of Ferrocenyl(2,2′-dipyrro)methane and Benzaldehyde. A mixture of 0.33 g (0.001 mol) of ferrocenyl(2,2′-dipyrro)methane,[22] 0.11 g (0.001 mol) of benzaldehyde, and 0.038 mL (0.0003 mol) of $BF_3 \cdot Et_2O$ in CH_2Cl_2 (150 mL) was reacted for 20 h at room temperature in argon atmosphere. After this period, 0.98 g (0.004 mol) of chloranil was added, and the resulting mixture was refluxed for 3.5 h. After solvent evaporation, the residue was chromatographied first on activity I alumina to eliminate the majority of the linear oligomeric reaction byproduct. After this step, reaction products were investigated using several sets of preparative silica gel TLC plates with a toluene−hexane−triethylamine mixture (69:29:2 v/v) as the eluent. It was found that because of the scrambling reaction, all possible cross-condensation products (i.e., H_2TPP, H_2FcPh$_3$P, *cis*-$H_2Fc_2Ph_2P$, *trans*-$H_2Fc_2Ph_2P$, H_2Fc_3PhP, and H_2TFcP) are formed in the reaction.

Results

Synthesis. The easiest synthetic pathway for preparation of the target asymmetric ferrocenyl-containing porphyrins is a well-known mixed-condensation reaction between ferrocenecarboxaldehyde, benzaldehyde, and pyrrole (Scheme 1).[23] As expected, all six possible porphyrin isomers (i.e., H_2TPP, H_2FcPh$_3$P, *cis*-$H_2Fc_2Ph_2P$, *trans*-$H_2Fc_2Ph_2P$, H_2Fc_3PhP, and H_2TFcP) were isolated from the reaction under cross-condensation conditions.[1o] Since the inner NH protons in the pure target porphyrins are located farthest upfield in the ^{1}H NMR spectrum of the reaction mixture (see discussion below), it is possible to estimate the initial porphyrin distribution by ^{1}H NMR spectroscopy (Supporting Information Figure 3). NMR data clearly indicate that the product distribution is close to statistical, suggesting only minor electronic influences of the phenyl and ferrocenyl substituents during formation of these asymmetric porphyrins.

Since it is expected (and was confirmed by NMR spectroscopy and product isolation) that the statistical yield of the *trans*-$H_2Fc_2Ph_2P$ complex should be the smallest out of all other asymmetric ferrocenyl-containing porphyrins (i.e., H_2FcPh$_3$P, *cis*-$H_2Fc_2Ph_2P$, *trans*-$H_2Fc_2Ph_2P$, and H_2Fc_3-PhP), we also attempted to prepare this specific compound using the reaction between ferrocenyl(2,2′-dipyrro)methane and benzaldehyde. This synthetic approach in the absence of the scrambling reaction should result in formation of the single reaction product (*trans*-$H_2Fc_2Ph_2P$). Similar to earlier mentioned cross-condensation reactions between dipyrromethane, ferrocenyl(2,2′-dipyrro)methane, and benzaldehyde as well as phenyl(2,2′-dipyrro)methane and cymantrenylcarboxaldehyde,[22] the reaction between ferrocenyl(2,2′-dipyrro)methane and benzaldehyde again results

(22) (a) Loim, N. M.; Abramova, N. V.; Khaliullin, R. Z.; Lukashov, Y. S.; Vorontsov, E. V.; Sokolov, V. I. *Russ. Chem. Bull.* **1998**, *47*, 1016–1020. (b) Gostev, F. E.; Nadtochenko, V. A.; Sarkisov, O. M.; Loim, N. M.; Abramova, N. V.; Chirvonyi, V. S. *Khim. Fiz.* **2004**, *23*, 3–14. (c) Auger, A.; Muller, A. J.; Swarts, J. C. *Dalton Trans.* **2007**, 3623–3633.

(23) (a) Lindsey, J. S. In *The Porphyrin Handbook*; Academic Press: New York, 2000; Vol *1*; pp 45−118. (b) Smith, K. M.; Vicente, M. G. H. In *Science of Synthesis*; Georg Thieme Verlag: Stuttgart, Germany, 2004; Vol. *17*, pp 1081−1235. (c) Cavaleiro, J. A. S.; Tome, A. C.; Neves, M. G. P. M. S. In *Handbook of Porphyrin Science*; Kadish, K. K., Smith, K. M., Guilard, R., Eds.; World Scientific: Singapore, 2010; Vol. *2*, pp 193 − 294.

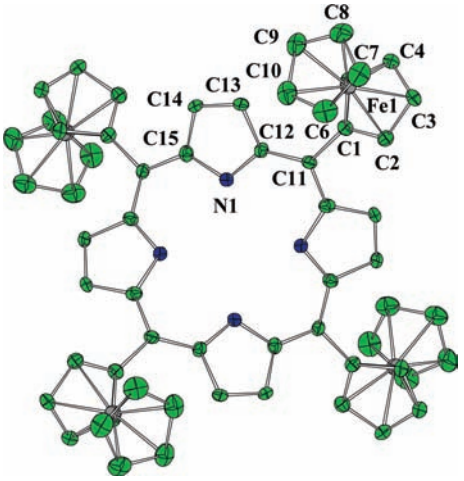

Figure 1. X-ray crystal structure of H_2TFcP at 50% probability level. All hydrogen atoms are omitted for clarity.

in the formation of H_2TPP, H_2FcPh$_3$P, *cis*-$H_2Fc_2Ph_2P$, *trans*-$H_2Fc_2Ph_2P$, H_2Fc_3PhP, and H_2TFcP compounds, making purification of the target *trans*-$H_2Fc_2Ph_2P$ quite a challenging task. Unlike several ferrocenyl-containing porphyrins, mentioned earlier,[11] the separation of the H_2TPP, H_2FcPh$_3$P, *cis*-$H_2Fc_2Ph_2P$, *trans*-$H_2Fc_2Ph_2P$, H_2Fc_3PhP, and H_2TFcP compounds requires a combination of column chromatography and preparative TLC methods (Supporting Information Figure 4) to obtain spectroscopically pure compounds.

Geometry and Electronic Structure. In the absence of X-ray data on target asymmetric compounds, their geometries and electronic structures were investigated using a DFT approach, tested first on the H_2TFcP complex for which the geometry was determined by X-ray crystallography (Figure 1, Experimental Section, and Supporting Information Table 1). It was found that the bond distances, angles, and torsion angles in H_2TFcP are reproduced well by the DFT approach described in the Experimental Section. This is in agreement with reports on the calculation of the electronic structures and properties of the other small ferrocenyl-containing compounds.[24] The DFT- predicted electronic structures and geometries of H_2TPP, H_2FcPh$_3$P, *trans*-$H_2Fc_2Ph_2P$, *cis*-$H_2Fc_2Ph_2P$, H_2Fc_3PhP, and H_2TFcP are compared in Figures 2−4 and Supporting Information Table 1.

In all cases, phenyl substituents were found to be nearly perpendicular to the porphyrin core, while the Cp rings were found to have a torsion angle with the porphyrin ring between 41.6° and 46.1° (Supporting Information Table 1). The lowest energy DFT predicted geometry of H_2TFcP corresponds to the α,*β*,α,*β*-H_2TFcP atropisomer,

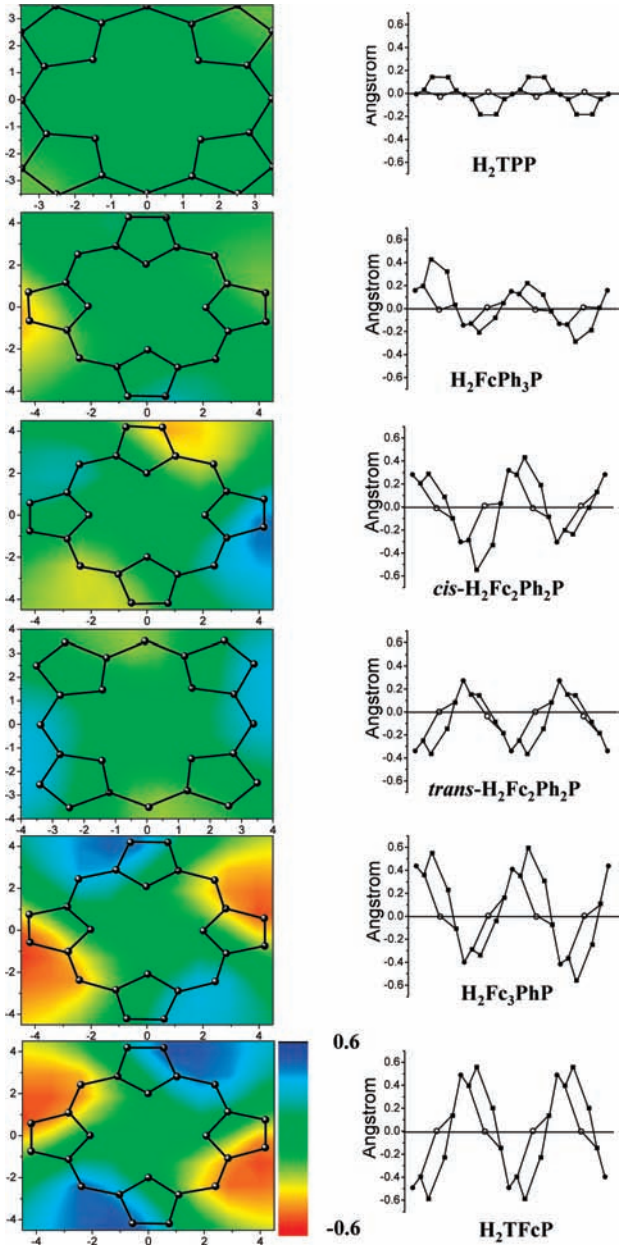

Figure 2. 2D counterplot analyses of nonplanarity in ferrocenyl-containing porphyrins as compared to H_2TPP. In all cases, four internal nitrogen atoms are used as the reference plane.

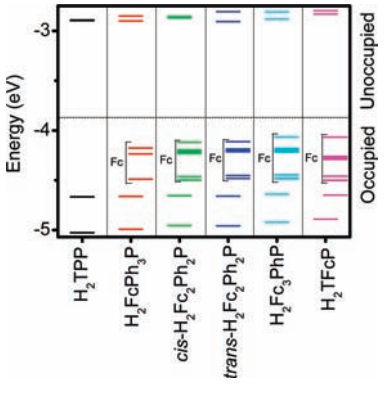

Figure 3. Partial molecular orbital diagram for ferrocenyl-containing porphyrins and H_2TPP predicted at the DFT level. Predominantly ferrocene-based orbitals are labeled as Fc.

(24) (a) Semencic, M. C.; Heinze, K.; Foerster, C.; Rapic, V. *Eur. J. Inorg. Chem.* **2010**, 1089–1097. (b) Roy, L. E.; Jakubikova, E.; Guthrie, M. G.; Batista, E. R. *J. Phys. Chem. A* **2009**, *113*, 6745–6750. (c) Romero, T.; Caballero, A.; Espinosa, A.; Tarraga, A.; Molina, P. *Dalton Trans.* **2009**, 2121–2129. (d) Helten, H.; Fankel, S.; Feier-Iova, O.; Nieger, M.; Espinosa Ferao, A.; Streubel, R. *Eur. J. Inorg. Chem.* **2009**, 3226–3237. (e) Pinjari, R. V.; Gejji, S. P. *J. Phys. Chem. A* **2008**, *112*, 12679–12686. (f) Fuentealba, M.; Garland, M. T.; Carrillo, D.; Manzur, C.; Hamon, J.-R.; Saillard, J.-Y. *Dalton Trans.* **2008**, 77–86. (g) Nemykin, V. N.; Maximov, A. Y.; Koposov, A. Y. *Organometallics* **2007**, *26*, 3138. (h) Nemykin, V. N.; Makarova, E. A.; Grosland, J. O.; Hadt, R. G.; Koposov, A. Y. *Inorg. Chem.* **2007**, *46*, 9591. (i) Herber, R. H.; Nowik, I.; Grossland, J. O.; Hadt, R. G.; Nemykin, V. N. *J. Organomet. Chem.* **2008**, *693*, 1850. (j) Nemykin, V. N.; Hadt, R. G. *Inorg. Chem.* **2006**, *45*, 8297–8307.

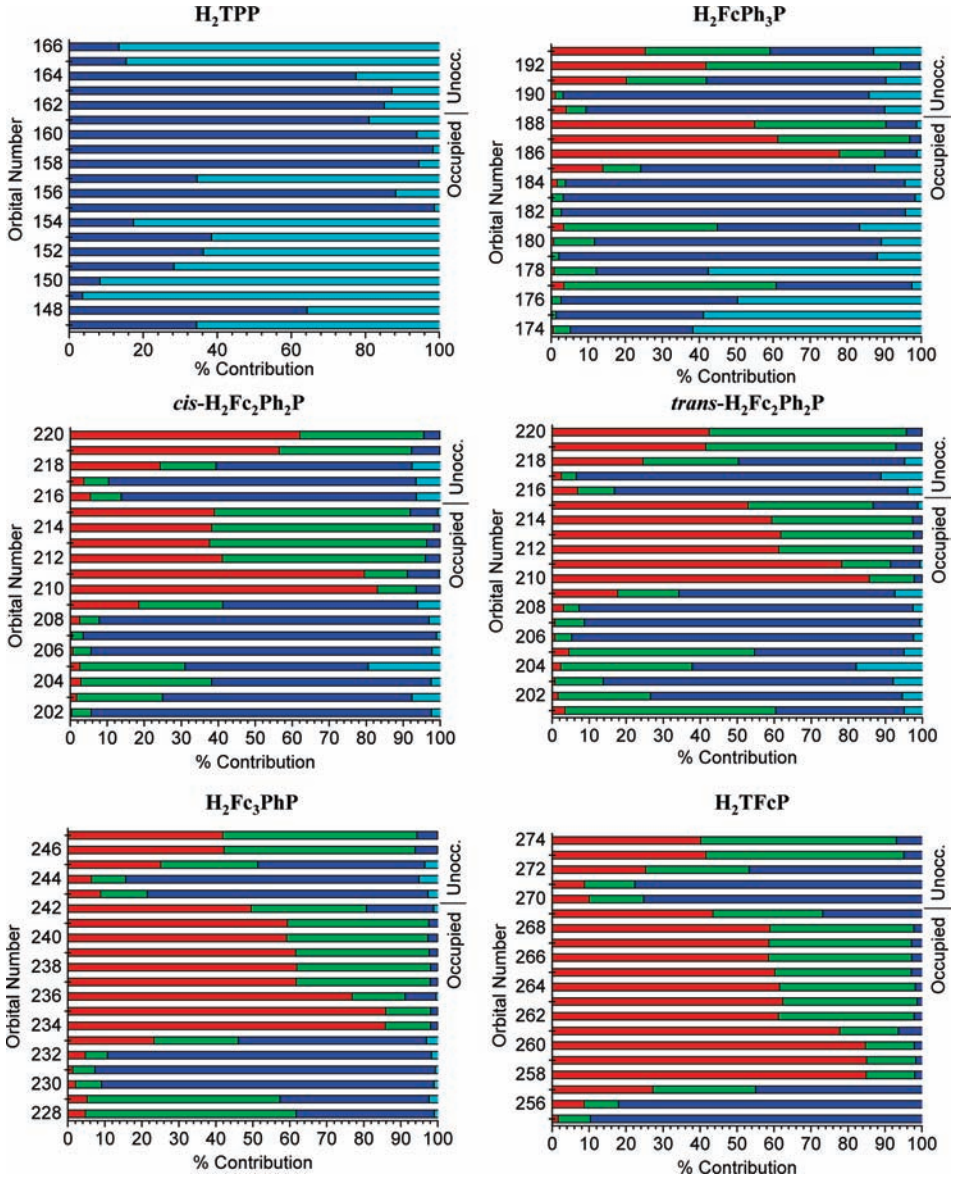

Figure 4. Molecular orbital compositions for frontier orbitals in ferrocenyl-containing porphyrins and H_2TPP predicted at the DFT level. Contributions from iron AOs are in red, cyclopentadienyl ligands are in green, porphyrin core is in blue, and phenyl substituents are in cyan.

in excellent agreement with the X-ray data. The lowest energy atropoisomers of H_2Fc_3PhP and *cis*-$H_2Fc_2Ph_2P$ were found to be α,*β*,α-H_2Fc_3PhP and α,*β*-*cis*-$H_2Fc_2Ph_2P$, respectively. The lowest energy structure of the *trans*-$H_2Fc_2Ph_2P$ compound corresponds to the α,α-*trans*-$H_2Fc_2Ph_2P$ atropisomer. This arrangement of ferrocene substituents is in agreement with α,*β*,α,*β*-H_2Fc_4P and α,*β*,α-H_2Fc_3PhP because the ferrocenyl groups located at the *meso*-positions are "α" in these complexes, and a similar atropisomer formation was observed for the other reported 5,15-bis(ferrocenyl)porphyrins.[1c,e] The α,α arrangement of the ferrocene groups on *trans*-$H_2Fc_2Ph_2P$ appeared to distort the N_4 plane on the porphyrin ring slightly less than the α,*β* arrangement of ferrocenyl substituents in *cis*-$H_2Fc_2Ph_2P$ (Figure 2). In general, the degree of nonplanarity of the porphyrin core increases as more ferrocene groups replace phenyl substituents at *meso* positions. Indeed, the DFT predicted average displacements from the N_4 plane of the porphyrin core are H_2TPP, 0.071 Å; H_2FcPh_3P, 0.1281 Å; *trans*-$H_2Fc_2Ph_2P$, 0.1688 Å; *cis*- $H_2Fc_2Ph_2P$, 0.2037 Å; H_2Fc_3PhP, 0.2509 Å; and H_2TFcP, 0.3031 Å.

The molecular orbital diagrams for H_2TPP, H_2FcPh_3P, *trans*-$H_2Fc_2Ph_2P$, *cis*-$H_2Fc_2Ph_2P$, H_2Fc_3PhP, and H_2TFcP are presented in Figure 3, with an analysis of the orbital composition in Figure 4. Frontier orbitals of the target compounds are pictured in Supporting Information Figure 5. Symmetry lowering in metal-free porphyrins removes any orbital degeneracy. However, near-degenerate molecular orbitals can be clearly seen. In agreement with Gouterman's classic four orbital model for porphyrins,[25] the HOMO and HOMO−1 in H_2TPP are porphyrin-based π orbitals, which correspond to a_{1u} and a_{2u} MOs in common D_{4h} point group notation. The introduction of a single ferrocene substituent onto the porphyrin core in H_2FcPh_3P results in HOMO to

(25) (a) Gouterman, M. In *Porphyrins*; Dolphin, D. Ed.; Academic: New York, 1978; Vol. *3*, pp 1−165. (b) Gouterman, M. *J. Mol. Spectrosc.* **1961**, *6*, 138–163.

HOMO−2 becoming predominantly iron-centered (d_{xy}, $d_{x^2-y^2}$, and d_{z^2}) MOs while the classic porphyrin core-centered occupied π orbitals are located at lower energies. Similarly, six predominantly ferrocene centered MOs were observed as HOMO to HOMO−5 in *cis*-$H_2Fc_2Ph_2P$ and *trans*-$H_2Fc_2Ph_2P$ (three MOs per ferrocene substituent), nine predominantly ferrocene centered MOs were observed as HOMO to HOMO−8 in H_2Fc_3PhP, and 12 predominantly ferrocene centered MOs were observed as HOMO to HOMO−11 in H_2TFcP (Figures 3 and 4). The presence of predominantly ferrocene based HOMOs in ferrocenyl-containing porphyrins was further probed and confirmed by electrochemical data discussed below. In general, the energy of the predominantly ferrocene-based HOMO increases upon an increase in the number of ferrocene substituents with agreement with electrochemical data. In agreement with the previous computational data,[1q] the LUMO and LUMO+1 are almost degenerate and mainly porphyrin based π^* orbitals. In all cases, these MOs are energetically well separated from higher energy unoccupied orbitals (LUMO+2 and above). Again, the DFT predicted energy of LUMO follows the general trend in electrochemically observed reduction potentials.

NMR Spectroscopy. It is well-known that the porphyrin ring current in metal-free porphyrins significantly shields NMR signals of the inner NH protons, which usually can be observed in the negative region of the ^{1}H NMR δ scale.[26] Moreover, it has been suggested that the degree of nonplanarity of the porphyrin core can significantly affect the porphyrin ring current and thus the shielding of inner NH protons.[1o,26b,c] In agreement with this hypothesis, the signals for the inner NH protons become progressively less shielded when the number of ferrocene substituents increases (Supporting Information Figure 1A). The less shielded NH proton signals are consistent with the DFT-predicted degree of nonplanarity, which decreases π-orbital overlap in the porphyrin core and decreases the π current inside the porphyrin ring as more ferrocene substituents are added to the porphyrin core. Indeed, a linear correlation between the average deviation from the N4 plane and the position of NH signals in ^{1}H NMR spectra of these porphyrins can be clearly seen (Figure 5). In H_2Fc_3PhP, it is expected that the adjacent (with respect to phenyl ring) ferrocene substituents will be slightly different compared to that in the opposite (with respect to phenyl ring) location. In agreement with this expectation, the protons of the substituted Cp ring (α-Cp, β-Cp) and unsubstituted Cp ring (CpH) were observed as two nonequivalent sets (2:1 ratio) in H_2Fc_3PhP with α-Cp and CpH signals for adjacent (with respect to phenyl ring) ferrocene substituents less shielded as compared to those for the opposite (with respect to phenyl ring) ferrocene group (Supporting Information Figure 1B). In all other cases, as expected, only one set of ferrocene signals has been observed at room temperature, supporting the equivalence of ferrocene substituents. Signals of β-pyrrolic protons in ferrocenyl-containing porphyrins

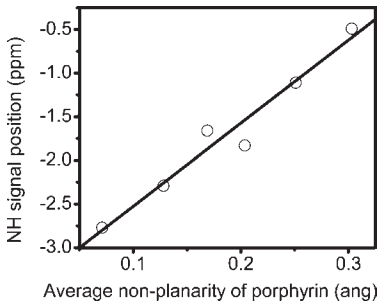

Figure 5. Correlation (r = 0.978) between degree of nonplanarity of the porphyrin core and NH signal position in ^{1}H NMR spectra of ferrocenyl-containing porphyrins.

follow a similar trend observed for NH protons, i.e., the larger the distortion of the local environment, the more downfield the signals are. Variable-temperature ^{1}H NMR experiments reveal free rotation of ferrocene substituents around the $C(Fc_{ipso})-C_{meso}$ bond in all target porphyrins at room temperature, in agreement with that observed earlier in H_2TFcP and *cis*-$H_2Fc_2Ph_2P$.[1o] A detailed analysis of the data will be provided in a separate publication.

Mass Spectra. The protonated molecular ions dominated the APCI spectra of all investigated porphyrins (Supporting Information Figure 2), which is consistent with the earlier reported APCI data on transition-metal ferrocenyl-containing MTFcP and the other porphyrins.[1o,q,27] Representative collision-induced dissociation[28] data for H_2FcPh_3P, *cis*-$H_2Fc_2Ph_2P$, *trans*-$H_2Fc_2Ph_2P$, and H_2Fc_3PhP are shown in Supporting Information Figure 2 and compared to the known H_2TFcP. In all cases, APCI-MS/MS reveals similar patterns to the H_2TFcP and MTFcP compounds investigated earlier. In particular, the fragmentation pattern associated with a loss of a cyclopentadiene ring, a ferrocene group, or a combination of both has been observed. For instance, the fragmentation pattern for H_2FcPh_3P included $[M-Cp]^+$ and $[M-Fc]^+$ peaks (Supporting Information Figure 2). Along with $[M-Cp]^+$, the H_2Fc_3PhP fragmentation pattern contained $[M-2Cp]^+$, $[M-Fc]^+$, $[M-Fc-Cp]^+$, $[M-Fc-2Cp]^+$, $[M-2Fc]^+$, and $[M-2Fc-Cp]^+$ (Supporting Information Figure 2). In addition to the fragmentation experiments, high-resolution ESI experiments were conducted in order to confirm elemental composition of the target compounds (Supporting Information Figure 2). In all cases, excellent agreement between theory and experiment has been observed.

UV−vis−NIR and MCD Spectroscopy of Neutral Compounds. The UV−vis−NIR and MCD spectra of neutral H_2TPP, H_2FcPh_3P, *trans*-$H_2Fc_2Ph_2P$, *cis*-$H_2Fc_2Ph_2P$, H_2Fc_3PhP, and H_2TFcP (Figure 6) are characteristic of

(26) (a) Friebolin, H. *Basic one- and two-dimensional NMR spectroscopy*, 4th ed.; Wiley-VCH: New York, 2005; pp 305−334. (b) Cheek; J. H. D. In *Porphyrin Handbook*; Kadish, K. M., Smith, K. M., Guillard, R., Eds.; Academic Press: New York, 2000; Vol. 7, pp 339−369. (c) Cheng, R.-J.; Chen, Y.-R.; Chen, C.-C. *Heterocycles* **1994**, *38*, 1465–1469. (d) Smith, K. M.; Abraham, R. J.; Pearson, H. *Tetrahedron* **1982**, *38*, 2441–2449.

(27) (a) Van Berkel, G. J.; McLuckey, S. A.; Glish, G. L. *Anal. Chem.* **1991**, *63*, 1098–1109. (b) Domingues, M. R. M.; Marques, M. G. O. S.; Domingues, P.; Neves, M. G.; Cavaleiro, J. A. S.; Ferrer-Correia, A. J.; Nemirovskiy, O. V.; Gross, M. L. *J. Am. Soc. Mass Spectrom.* **2001**, *12*, 381–384. (c) Lau, K. S. F.; Sadilek, M.; Gouterman, M.; Khalil, G. E.; Brückner, C. *J. Am. Soc. Mass Spectrom.* **2006**, *17*, 1306–1314. (d) Serra, V. V.; Domingues, M. R. M.; Faustino, M. A. F.; Domingues, P.; Tomė, J. P. C.; Neves, M. G. P. M. S.; Tomė, A. C.; Cavaleiro, J. A. S.; Ferrer-Correia, A. J. *Rapid Commun. Mass Spectrom.* **2005**, *19*, 2569–2580.

(28) (a) Nemykin, V. N.; Basu, P. *Inorg. Chim. Acta* **2005**, *358*, 2876–2882. (b) Nemykin, V. N.; Basu, P. *Dalton Trans.* **2004**, 1928–1933. (c) Butcher, C. P. G.; Dyson, P. J.; Johnson, B. F. G.; Khimyak, T.; McIndoe, J. S. *Chem.—Eur. J.* **2003**, *9*, 944–950. (d) Crawford, E.; Dyson, P. J.; Forest, O.; Kwok, S.; McIndoe, J. S. *J. Cluster Sci.* **2006**, *17*, 47–63.

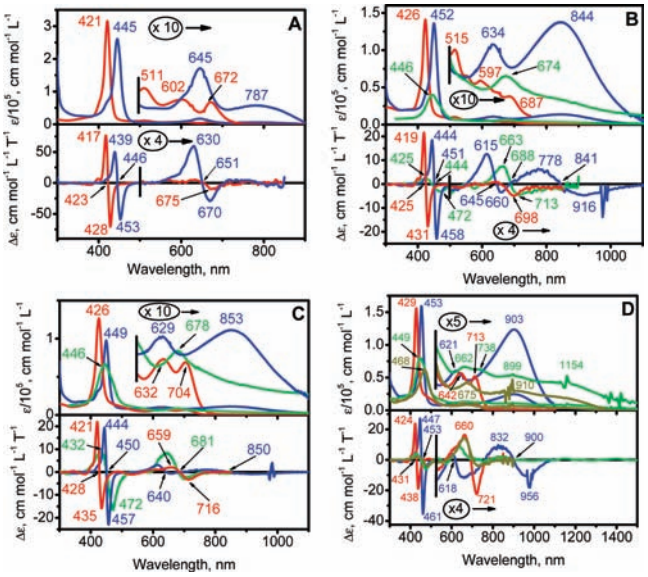

Figure 6. UV−vis and MCD spectra of (A) H_2FcPh_3P (red) and $[H_2FcPh_3P]^+$ (blue); (B) *cis*-$H_2Fc_2Ph_2P$ (red), [*cis*-$H_2Fc_2Ph_2P]^+$ (blue), and [*cis*-$H_2Fc_2Ph_2P]^{2+}$ (green); (C) *trans*-$H_2Fc_2Ph_2P$ (red), [*trans*-$H_2Fc_2Ph_2P]^+$ (blue), and [*trans*-$H_2Fc_2Ph_2P]^{2+}$ (green); (D) H_2Fc_3PhP (red), $[H_2Fc_3PhP]^+$ (blue), $[H_2Fc_3PhP]^{2+}$ (green), and $[H_2Fc_3PhP]^{3+}$ (dark yellow).

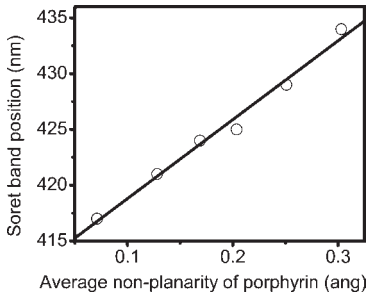

Figure 7. Correlation ($r = 0.993$) between degree of nonplanarity of the porphyrin core and Soret band position in UV−vis spectra of ferrocenyl-containing porphyrins.

metal-free porphyrins[29] and dominated by the Soret band located at 417, 421, 424, 425, 429, and 434 nm, respectively. The Soret band, in all cases, is represented by a Faraday pseudo-*A* term in their respective MCD spectra. Subsequent replacement of phenyl groups with ferrocenyl groups at *meso* positions resulted in the red-shift in the Soret band maxima, probably due to increased nonplanarity of the porphyrin core. Similar to the correlation between the NH signal position and the degree of porphyrin core nonplanarity (*vide supra*), there exists a linear correlation between the Soret band maxima and the degree of nonplanarity of the porphyrin core (Figure 7).

(29) Cheek; J.; Dawson, J. H. In *Porphyrin Handbook*; Kadish, K. M., Smith, K. M., Guillard, R., Eds.; Academic Press: New York, 2000; Vol. *7*, pp 339 − 369.

(30) (a) Mack, J.; Asano, Y.; Kobayashi, N.; Stillman, M. J. *J. Am. Chem. Soc*. **2005**, *127*, 17697–17711. (b) Medforth, C. J.; Smith, K. M. *Tetrahedron Lett*. **1990**, *31*, 5583–55866. (c) Shelnutt, J. A.; Majumder, S. A.; Sparks, L. D.; Hobbs, J. D.; Medforth, C. J.; Senge, M. O.; Smith, K. M.; Miura, M.; Luo, L.; Quirke, J. M. E. *J. Raman Spectrosc*. **1992**, *23*, 523–529. (d) Haddad, R. E; Gazeau, S.; Pecaut, J.; Marchon, J.-C.; Medforth, C. J; Shelnutt, J. A. *J. Am. Chem. Soc*. **2003**, *125*, 1253–1268. (e) Subbotin, N. B.; Nemykin, V. N.; Voloshin, Y. Z. *Mendeleev Commun*. **1993**, 121. (f) Nemykin, V. N.; Kobayashi, N.; Mytsyk, V. M.; Volkov, S. V. *Chem. Lett*. **2000**, 546.

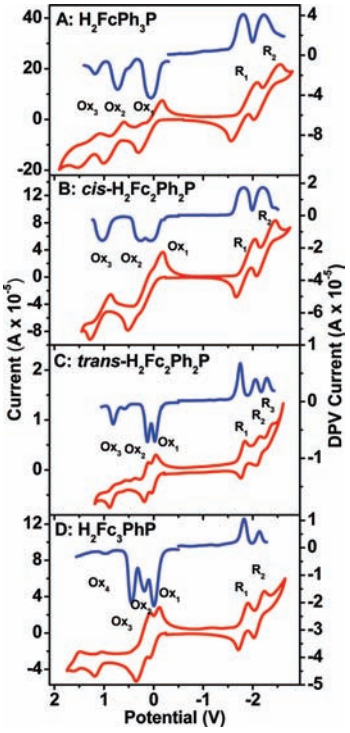

Figure 8. CV (bottom) and DPV (top) data on ferrocenyl-containing porphyrins in the DCM/TFAB system.

Another interesting observation is that the intensity of the Soret band also decreases with the degree of nonplanarity of the porphyrin core, which can be explained by the decrease of p−p orbital overlap as a function of porphyrin core nonplanarity. Similar observations have been reported for nonplanar porphyrins and phthalocyanines.[30] The Q-band region also follows the decreasing-energy trend as more ferrocenyl groups replace phenyl groups on the porphyrin core. All Q bands (~600−700 nm) of the poly(ferrocenyl)-poly(phenyl)-porphyrins are represented by two Faraday *B* terms in the MCD spectra. The positive Faraday *B* term is observed for the higher energy Q_y, and a negative Faraday *B* term is observed for the lower energy Q_x bands, which is typical for *meso*-substituted porphyrins.

Redox Properties of *meso*-Ferrocenyl-Containing Porphyrins. It has been suggested that the best electrolyte/solvent combination for studying polyferrocenyl-containing complexes should consist of a low dielectric constant solvent and a noncoordinating electrolyte in order to minimize the influence of electrostatic, magnetic inductive, static, and electronic coupling factors on electron-transfer processes and $\Delta E_{1/2}$ values in multinuclear transition-metal complexes.[11] Following this idea, the redox properties of H_2FcPh_3P, *trans*-$H_2Fc_2Ph_2P$, *cis*-$H_2Fc_2Ph_2P$, and H_2Fc_3PhP were investigated by CV, DPV, and SWV methods using low polarity DCM as a solvent and a weakly coordinating TFAB electrolyte with the CV and DPV results shown in Figure 8 and redox potentials listed in Table 1. It has been found that within a solvent electrochemical window, all observed redox processes in the target porphyrins exhibited quasi-reversible behavior. In all cases, ferrocene-based oxidation was observed between porphyrin-centered oxidation and reduction waves. The separation between the porphyrin core-centered first ring oxidation and first ring reduction processes

Table 1. Summary of Electrochemical (DPV) Data for Ferrocenyl-Containing Porphyrins in a DCM/TFAB System[a]

Process[b]	Ox_5	Ox_4	Ox_3	Ox_2	Ox_1	R_1	R_2	R_3
H_2FcPh_3P			1.19 (P)	0.72 (P)	0.06 (Fc)	−1.79	−2.22	
cis- $H_2Fc_2Ph_2P$			1.00 (P)	0.24 (Fc)	0.04 (Fc)	−1.82	−2.20	
trans- $H_2Fc_2Ph_2P$			0.84 (P)	0.15 (Fc)	0.00 (Fc)	−1.78	−2.10	−2.30
H_2Fc_3PhP		0.97 (P)	0.43 (Fc)	0.17 (Fc)	−0.02 (Fc)	−1.81	−2.13	
H_2TFcP	1.42 (P)	0.34 (Fc)	0.24 (Fc)	0.15 (Fc)	−0.07 (Fc)	−1.78	−2.06	

[a] All potentials are referenced to the Fc/Fc^+ couple. [b] P = porphyrin-centered process, Fc = ferrocene-centered process, Ox = oxidation, R = reduction. All reductions are porphyrin core centered.

was found to be a larger than the typical separation observed in tetra-*meso*-arylsubstituted porphyrins (~2.4 V)[31] and was attributed to the presence of redox active ferrocene MOs located at higher energy than the porphyrin-based π orbitals. The first two reductions in the target compounds were both assigned to the reduction of the porphyrin ring due to ferrocene's stability toward reduction. The difference between the first and second reduction potentials is similar to H_2TPP, although reduction potentials were found to be more negative and were located at around −1.8 V and −2.2 V for all molecules studied (Figure 8, Table 1). In addition, *trans*-$H_2Fc_2Ph_2P$ had a third ring reduction observed at −2.82 V. The first oxidation at 0.064 V for H_2FcPh_3P (Figure 8A, Table 1) was attributed to a ferrocene-based oxidation followed by two porphyrin ring oxidations at 0.718 and 1.186 V respectively, which are in the range of previously reported monosubstituted ferrocenylporphyrins. In the DCM/TFAB system, the first two oxidations in *cis*-$H_2Fc_2Ph_2P$ (Figure 8B, Table 1) were observed at 0.036 and 0.244 V and were attributed to the stepwise oxidation of ferrocene substituents. The porphyrin ring oxidation was observed at 1.004 V, which is in the range of similar porphyrin systems. The oxidation of *trans*-$H_2Fc_2Ph_2P$ (Figure 8C, Table 1) was similar to that of *cis*-$H_2Fc_2Ph_2P$ with the stepwise ferrocene-based oxidations observed at 0.000 V and 0.150 V and the porphyrin oxidation wave observed at 0.842 V.

The successive removal of individual electrons from the ferrocene substituents confirms the long-distance metal−metal coupling in both *cis*- and *trans*-$H_2Fc_2Ph_2P$ complexes, which was further supported by the spectroelectrochemical and chemical oxidation experiments discussed below. Separation between the first two redox waves of *cis*- and *trans*-$H_2Fc_2Ph_2P$ are 208 mV and 150 mV, respectively. The comproportionation constants calculated for the $H_2Fc_2Ph_2P + [H_2Fc_2Ph_2P]^{2+} \leftrightarrows [H_2Fc_2Ph_2P]^{+}$ process for both *cis*- and *trans*-$H_2Fc_2Ph_2P$ are relatively large (3300 for *cis*- and 340 for *trans*-$H_2Fc_2Ph_2P$; Table 2), suggesting the possible formation of the corresponding mixed-valence species in the DCM/TFAB system. Although comproportionation constants for both *cis*- and *trans*-$H_2Fc_2Ph_2P$ complexes are large enough to form stable species, the value for *cis*-$H_2Fc_2Ph_2P$ more closely resembles that of H_2TFcP, indicating that the ferrocenium substituents in $[H_2TFcP]^{2+}$ are likely to be located between adjacent 5,10-*meso* potitions in the porphyrin core.

The first oxidation of H_2Fc_3PhP appears negative relative to ferrocene (Figure 8D, Table 1), which is similar to the first oxidation H_2TFcP.[1r] Oxidations of individual ferrocene moieties of H_2Fc_3PhP are well-separated (ΔE_{1-2} ~190 mV, ΔE_{2-3} ~270 mV) and were observed at −0.018 V, 0.168 V, and 0.434 V. The porphyrin ring oxidation of H_2Fc_3PhP was observed at 0.972 V. Polyferrocenyl porphyrin systems offer unique insight into how oxidations occur in $[H_2TFcP]$. The two processes compete in the formation of $[H_2TFcP]^{2+}$ and $[H_2Fc_3PhP]^{2+}$: the oxidation of the second iron atom at an adjacent or opposite position relative to the position of the iron atom that was oxidized first. Two processes are conceivable for the oxidation of the third iron atom in $[H_2Fc_3PhP]^{3+}$ and $[H_2TFcP]^{3+}$. The doubly charged precursor may have the charges located at adjacent or opposite positions, $[H_2Fc_3PhP]^{2+}$ and $[H_2TFcP]^{2+}$, which leads to oxidation processes to form $[H_2Fc_3PhP]^{3+}$ and $[H_2TFcP]^{3+}$. The lower first oxidation potential of *trans*-$H_2Fc_2Ph_2P$ suggests that the opposite oxidation starts to occur first because the iron atoms have a greater distance between them and therefore less communication, but statistically the oxidation of the adjacent substituent in $[H_2Fc_3PhP]^{+}$ and $[H_2TFcP]^{+}$ is more favored. In addition to pure statistical possibilities, the energetics of the electronic isomers must be considered. Because of the slow time scale of the CV and DPV scans, an average of the adjacent and opposite oxidations is seen when multiple pathways are possible. As the first three ferrocenyl groups are added to the ring, the oxidations have large comproportionation constants (Table 2); it is not until the fourth ferrocenyl group is added that the separation between ferrocene-based oxidation waves decreases. The cumulative electron-donor effect of the ferrocene substituents shifts the first oxidation potential of H_2TFcP 130 mV more negative than that observed in H_2FcPh_3P. Although it is possible to classify all MV cations (i.e., $[cis\text{-}H_2Fc_2Ph_2P]^{+}$, $[trans\text{-}H_2Fc_2Ph_2P]^{+}$, $[H_2Fc_3PhP]^{+}$, and $[H_2Fc_3PhP]^{2+}$) using experimentally determined comproportionation constants, K_c, as class II spin-localized systems in Robin−Day classification,[32] Keene and D'Alessandro, Geiger and co-workers,

Table 2. Summary of Comproportionation Constants (Kc) in Ferrocenyl-Containing Porphyrins Estimated Using Electrochemical Data in the DCM/TFAB System

	$[P]^{2+} + P^0 \leftrightarrows 2[P]^{+}$	$[P]^{3+} + [P]^{+} \leftrightarrows 2[P]^{2+}$	$[P]^{4+} + [P]^{3+} \leftrightarrows 2[P]^{2+}$
cis-$H_2Fc_2Ph_2P$	3.28×10^3		
trans-$H_2Fc_2Ph_2P$	3.43×10^2		
H_2Fc_3PhP	1.39×10^3	3.13×10^4	
H_2TFcP	5.65×10^3	33	49

(31) (a) Kadish, K. M.; Morrison, M. M. *J. Am. Chem. Soc.* **1976**, *98*, 3326. (b) Kadish, K. M.; Caemelbecke, E. V.; Royal, G. In *Porphyrin Handbook*; Kadish, K. M., Smith, K. M., Guilard, R., Eds.; Academic Press: New York, 2000; Vol. *8*, pp 1−114.

(32) (a) Robin, M. B.; Day, P. *Adv. Inorg. Chem. Radiochem.* **1967**, *10*, 247. (b) Creutz, C. *Prog. Inorg. Chem.* **1983**, *30*, 1. (c) Hush, N. S. *Prog. Inorg. Chem.* **1967**, *8*, 391.

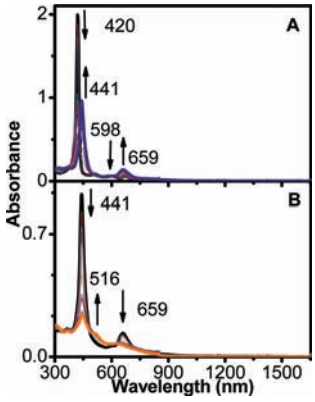

Figure 9. Oxidative transformations of H_2FcPh_3P into $[H_2FcPh_3P]^+$ (A) and $[H_2FcPh_3P]^{2+}$ (B) monitored by the spectroelectrochemical method.

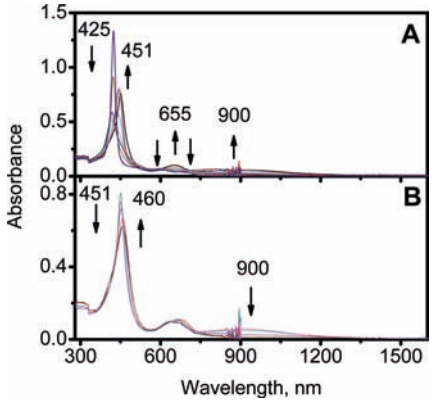

Figure 10. Transformations of *cis*-$H_2Fc_2Ph_2P$ into $[cis\text{-}H_2Fc_2Ph_2P]^+$ (A) and $[cis\text{-}H_2Fc_2Ph_2P]^{2+}$ (B) monitored by the spectroelectrochemical method.

and others[11,33] have cautioned against this method because the results are highly dependent on the polarity of the solvent and coordinating properties of the supporting electrolyte.

Spectroelectrochemistry of Ferrocenyl-Containing Porphyrins. Taking into consideration the separation between ferrocene-based oxidation waves in the target porphyrins, spectroelectrochemistry was used to obtain spectroscopic signatures of different oxidized species originating from the neutral compounds and were compared to the spectra of the chemically oxidized species. The spectroelectrochemical transformation of H_2FcPh_3P results in the formation of the $[H_2FcPh_3P]^+$ species accompanied by five isosbestic points and is presented in Figure 9A. During oxidation, the Soret band shifted from 420 to 441 nm with a loss in intensity. The Q bands at 598 nm 673 nm also disappeared and revealed a new band at 659 nm, characteristic of the charge-transfer band observed in ferrocenium cations. As expected, no intervalence charge transfer (IVCT) band, characteristic of mixed-valence compounds, was observed because only one iron center is present in $[H_2FcPh_3P]^+$. During a second transformation (Figure 9B), the Soret band and a LMCT band at 659 nm decrease with the growth of a prominent shoulder at 516 nm, corresponding to the formation of the $[H_2FcPh_3P]^{2+}$ species, in which Fe^{III} and a porphyrin-based cation radical are both present. During the first oxidation of *cis*-$H_2Fc_2Ph_2P$ (Figure 10A), the Soret and both Q-bands lost their intensities, and a new band at 655 nm appeared in the UV−vis spectrum. Characteristic of mixed-valence compounds, an IVCT band close to 900 nm was observed in $[cis\text{-}H_2Fc_2Ph_2P]^+$, confirming the ferrocene-based oxidation process. The oxidation of the second ferrocene substituent in $[cis\text{-}H_2Fc_2Ph_2P]^+$ results in the disappearance of the IVCT band at ~900 nm, a further loss of intensity of the Soret band, and the growth of the ferrocenium charge transfer band located at 655 nm (Figure 10B).

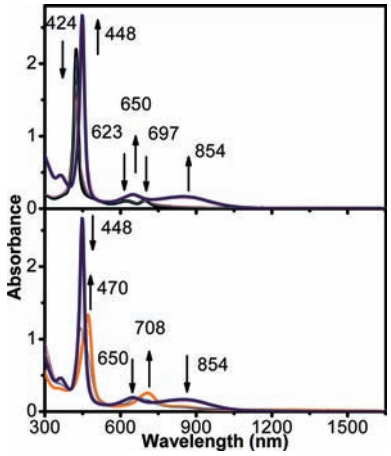

Figure 11. Oxidative transformations of *trans*-$H_2Fc_2Ph_2P$ into $[trans\text{-}H_2Fc_2Ph_2P]^+$ (A) and $[trans\text{-}H_2Fc_2Ph_2P]^{2+}$ (B) monitored by the spectroelectrochemical method.

The formation of the mixed-valence $[trans\text{-}H_2Fc_2Ph_2P]^+$ species under spectroelectrochemical conditions was accompanied by a red-shift in the Soret band from 424 to 448 nm, a loss of Q-band intensity at 623 nm and 697 nm, the appearance of the 650 nm band, and a characteristic IVCT band observed at 854 nm, supporting elimination of an electron from the ferrocene substituent (Figure 11A). The second one-electron oxidation of $[trans\text{-}H_2Fc_2Ph_2P]^+$ resulted in the disappearance of the IVCT band, along with the appearance of a band at 708 nm, and the shift of the Soret band to 470 nm (Figure 11B). As expected, the spectroelectrochemical generation of two mixed-valence species from H_2Fc_3PhP was observed.

The formation of the first mixed-valent $[H_2Fc_3PhP]^+$ species was accompanied by a Soret band shift and a loss in intensity, the disappearance of the Q-bands at 643 and 714 nm, and the appearance of the IVCT band observed at 936 nm (Figure 12A). The formation of the second mixed-valence species, $[H_2Fc_3PhP]^{2+}$, resulted in partial disappearance of the first IVCT band located at 936 nm and the appearance of the second broad IVCT band observed at ca. 1280 nm (Figure 12B). The formation of a new band located at 611 nm was also observed along with the shift of the Soret band to 408 nm and the formation of a prominent shoulder at 468 nm during the formation of $[H_2Fc_3PhP]^{2+}$.

(33) (a) D'Alessandro, D.; Keene, R. *Chem. Soc. Rev.* **2006**, *35*, 424. (b) D'Alessandro, D. M.; Keene, F. R. *Dalton Trans.* **2004**, 3950. (c) Southard, G. E.; Curtis, M. D. *Organometallics* **2001**, *20*, 508. (d) Yang, J.; Seneviratne, D.; Arbatin, G.; Andersson, A. M.; Curtis, J. C. *J. Am. Chem. Soc.* **1997**, 5329. (e) Neyhart, G. A.; Hupp, J. T.; Curtis, J. C.; Timpson, C. J.; Meyer, T. J. *J. Am. Chem. Soc.* **1996**, *118*, 3724. (f) Lau, K. W.; Hu, A. M.-H.; Yen, M. H.-J.; Fung, E. Y.; Grzybicki, S.; Matamoros, R.; Curtis, J. C. *Inorg. Chim. Acta* **1994**, *226*, 137.

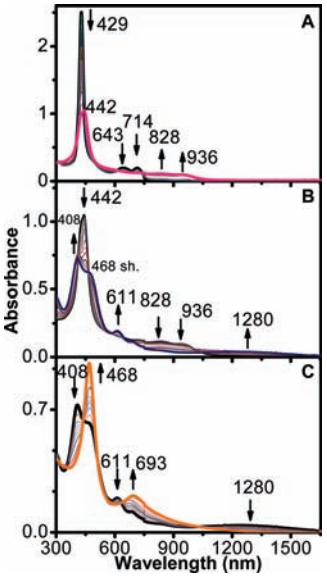

Figure 12. Oxidative transformations of H_2Fc_3PhP into $[H_2Fc_3PhP]^+$ (A), $[H_2Fc_3PhP]^{2+}$ (B), and $[H_2Fc_3PhP]^{3+}$ (C) monitored by the spectroelectrochemical method.

Subsequent removal of another electron from $[H_2Fc_3PhP]^{2+}$ resulted in the disappearance of the IVCT at ~1280 nm and the appearance of a new band at 693 nm and a new Soret band at 468 nm (Figure 12C). Overall, under spectroelectrochemical conditions (with the exception of H_2FcPh_3P), all target compounds studied can form ferrocene-centered mixed-valence species. Furthermore, the positions of the IVCT bands of the mixed-valence species formed are close to those reported during spectroelectrochemical oxidation of H_2TFcP, confirming that conformationally flexible substituents at distances longer than 12 Å are able to form mixed-valence species. It is also important to note that all oxidized compounds formed under spectroelectrochemical conditions showed complete reversibility and can be easily reduced to the corresponding starting neutral compounds by applying a small negative potential (Supporting Information Figure 6), similar to the electrochemical behavior observed for H_2TFcP.[1r]

UV−vis−NIR and MCD Spectra of Chemically Oxidized Mixed-Valence Compounds. Using the spectroscopic signatures obtained from spectroelectrochemistry, appropriate chemical oxidants were used to further probe the oxidized mixed-valence compounds by MCD spectroscopy. When silver triflate (AgOTf) was used as an oxidant, the final products were further probed by APCI MS to ensure that the silver ion was not incorporated into the porphyrin core during experiments. The $[H_2FcPh_3P]^+$ complex was formed by titration of the neutral compound with one equivalent of the oxidant, which yielded very similar results to spectroelectrochemistry (Figure 13). The Soret band at 421 nm decreased in intensity and shifted to 441 nm. The Q-bands at 601 and 670 nm disappeared, and a band at 678 nm resulting from a ferrocenium charge transfer appeared in the UV−vis spectrum.

No further changes in the UV−vis spectrum of $[H_2FcPh_3P]^+$ were observed when an excess of the AgOTf was used, in agreement with the oxidation potential of the Ag^+ ion in DCM and the position of the second oxidation

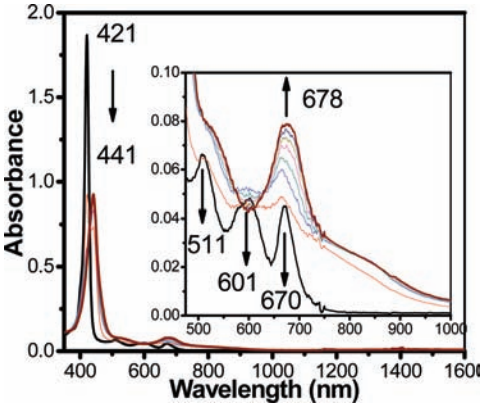

Figure 13. Formation of $[H_2FcPh_3P]^+$ by chemical oxidation.

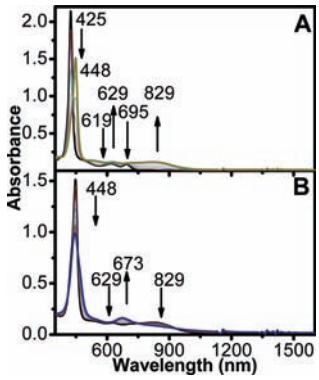

Figure 14. Chemical oxidation of *cis*-$H_2Fc_2Ph_2P$ into $[cis\text{-}H_2Fc_2Ph_2P]^+$ (A) and $[cis\text{-}H_2Fc_2Ph_2P]^{2+}$ (B).

potential of H_2FcPh_3P. As expected, no IVCT bands were present in the oxidized spectrum. The MCD spectrum of $[H_2FcPh_3P]^+$ consists of a Faraday pseudo-*A* term centered at 446 nm and two additional Faraday pseudo-*A* terms centered at 651 and 795 nm (Figure 6A). Similar to spectroelectrochemical experiments, the oxidation of *cis*-$H_2Fc_2Ph_2P$ with one equivalent of oxidant resulted in a red shift of the Soret band (from 425 to 448 nm), a disappearance of Q-bands at 619 and 695 nm, the appearance of a band at 629 nm, and a new IVCT band located at 829 (Figure 14A). Three Faraday pseudo-*A* terms centered ca. 451 nm (Soret), 635 nm (charge transfer), and 843 nm (IVCT) were observed in the MCD spectrum of $[cis\text{-}H_2Fc_2Ph_2P]^+$ (Figure 6B), which is consistent with the MCD signature of the mixed-valent $[H_2TFcP]^+$. The addition of a second equivalent of oxidant to $[cis\text{-}H_2Fc_2Ph_2P]^+$ results in a decrease of the intensity of the Soret band, the appearance of a new band at 673, and the disappearance of the IVCT band, suggesting the oxidation of both Fe^{II} centers to Fe^{III} (Figure 14B). In the MCD spectrum of $[cis\text{-}H_2Fc_2Ph_2P]^{2+}$, both of the major absorption bands are represented by MCD pseudo-*A*-terms centered at 443 and 690 nm (Figure 6B).

Formation of the mixed-valence *trans*-$[H_2Fc_2Ph_2P]^+$ was observed when *trans*-$H_2Fc_2Ph_2P$ oxidized with AgOTf as an oxidant, resulting in the appearance of an IVCT band at 831 nm, the disappearance of Q-bands at 619 and 698 nm, and a red-shift of the Soret band (from 424 to 447 nm, Figure 15A). The MCD spectrum of

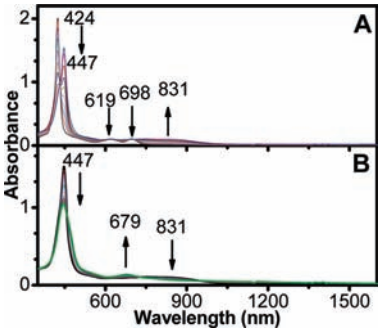

Figure 15. Chemical oxidation of *trans*-$H_2Fc_2Ph_2P$ into [*trans*-$H_2Fc_2Ph_2P$]$^+$ (A) and [*trans*-$H_2Fc_2Ph_2P$]$^{2+}$ (B).

trans-[$H_2Fc_2Ph_2P$]$^+$ (Figure 6C) is similar to that of [*cis*-$H_2Fc_2Ph_2P$]$^+$ with three MCD pseudo-*A* terms located at 450 (Soret band), 642 (LMCT band), and 831 nm (IVCT band). The addition of a second equivalent of oxidant resulted in the disappearance of the IVCT band, the appearance of a band at 679 nm, and an intensity decrease of the Soret band (Figure 15B). Again, the MCD spectrum of [*trans*-$H_2Fc_2Ph_2P$]$^{2+}$ consists of two Faraday pseudo-*A* terms (Figure 6C) similar to those observed in [*cis*-$H_2Fc_2Ph_2P$]$^{2+}$.

Two mixed-valence compounds were generated under chemical oxidation conditions in the case of the H_2Fc_3PhP complex. The first mixed-valence [H_2Fc_3PhP]$^+$ complex was prepared by the addition of one equivalent of oxidant. This resulted in a red-shift of the Soret band from 429 to 451 nm, the disappearance of Q-bands at 641 and 713 nm, and the appearance of an IVCT band at 888 nm (Figure 16A). The MCD spectrum of [H_2Fc_3PhP]$^+$ again revealed three MCD pseudo-*A* terms centered at 453 (Soret band), 618 (LMCT band), and 903 nm (IVCT band, Figure 6D). The addition of a second equivalent of oxidant to [H_2Fc_3PhP]$^+$ resulted in a decreased intensity of the initial IVCT band and the appearance of a second IVCT band at 1156 nm and a LMCT band at 657 nm (Figure 16B). The MCD spectrum of [H_2Fc_3PhP]$^{2+}$ is dominated by the Faraday pseudo-*A* term centered at the Soret band position (Figure 6D). Finally, the formation of [H_2Fc_3PhP]$^{3+}$ was accompanied by the disappearance of the IVCT band and a decrease in intensity of the Soret band (Figure 16C). The MCD spectrum of [H_2Fc_3PhP]$^{3+}$ is dominated by two Faraday pseudo-*A* terms centered at 460 and 656 nm (Figure 6D). Overall, the chemical oxidation data were in good agreement with the spectroelectrochemical experiments and the previously reported data on [H_2TFcP]$^{n+}$ compounds. The location and type of MCD signal of the IVCT band in the [*cis*-$H_2Fc_2Ph_2P$]$^+$, [*trans*-$H_2Fc_2Ph_2P$]$^+$, and [H_2Fc_3PhP]$^+$ species as well as the position of the IVCT band observed in [H_2Fc_3PhP]$^{2+}$ are similar to the analogous mixed valence species of [H_2Fc_4P]$^{n+}$, all of which were characterized by Mössbauer, XPS, and IR spectroscopy.

Traditionally, the Hush method is used by a majority of synthetic chemists to obtain the coupling element, H_{ab}, from experimental data.[33c] A more descriptive analysis of the intramolecular electron transfer characteristics in MV compounds, however, requires an intimate familiarization with the variation of the electronic energy as a function of nuclear coordinates.[33c]

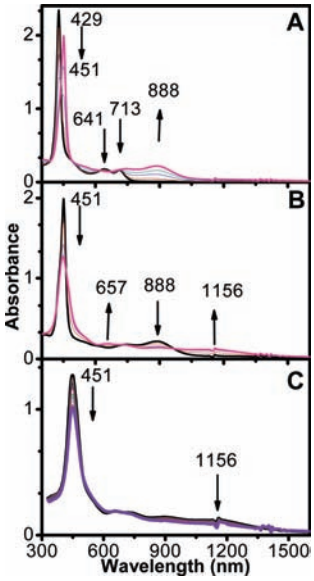

Figure 16. Chemical oxidation of H_2Fc_3PhP into [H_2Fc_3PhP]$^+$ (A), [H_2Fc_3PhP]$^{2+}$ (B), and [H_2Fc_3PhP]$^{3+}$ (C).

For instance, Schatz et al.[34] and Ondrechen and coworkers[35] have developed models to analyze MV dynamics in the Creutz-Taube ion.[36] Piepho's molecular orbital based method[37] has also been used. H_{ab} and α, the electronic coupling matrix element and delocalization parameter, respectively, can be estimated using eqs 1 and 2 and DFT predicted Fe−Fe distances in H_2TFcP and are displayed in Table 3.[33−38]

$$H_{ab} = 2.05 \times 10^{-2} \frac{(\nu_{max}\varepsilon_{max}\Delta\nu_{1/2})^{1/2}}{r_{ab}} \quad (1)$$

$$\alpha = 4.2 \times 10^{-4} \frac{\Delta\nu_{1/2}\varepsilon_{max}}{\nu_{max}r_{ab}^2} \quad (2)$$

where ν_{max} is the energy of the IVCT at band maximum in cm^{-1}, $\Delta\nu_{1/2}$ is the half-width at the band maximum in cm^{-1}, ε_{max} is the molar extinction coefficient of the IVCT, and r_{ab} is the distance between redox centers in Å. On the basis of the IVCT band energy, intensity, and width, the estimated H_{ab} and α values for [*cis*-$H_2Fc_2Ph_2P$]$^+$, [*trans*-$H_2Fc_2Ph_2P$]$^+$, [H_2Fc_3PhP]$^+$, and [H_2Fc_3PhP]$^{2+}$ complexes are in the range of valence-localized class II mixed-valence species in the Robin and Day classification, in agreement with earlier reported mixed-valence [H_2TFcP]$^{n+}$ compounds. The counterion dependence of the IVCT band maximum is also indicative of the formation of class II species as evidenced by oxidation using AgOTf, DDQ, or electrochemical conditions.

(34) (a) Piepho, S. B.; Krausz, E. R.; Schatz, P. N. *J. Am. Chem. Soc.* **1978**, *100*, 2996. (b) Wong, K. Y.; Schatz, P. N. *Prog. Inorg. Chem.* **1981**, *28*, 369.
(35) Zhang, L.-T; Ko, J.; Ondrechen, M. J. *J. Am. Chem. Soc.* **1987**, *109*, 1666.
(36) Creutz, C.; Taube, H. *J. Am. Chem. Soc.* **1969**, *91*, 3988.
(37) Piepho, S. B. *J. Am. Chem. Soc.* **1988**, *110*, 6319.
(38) Lever, A. B. P. *Inorganic Electronic Spectroscopy*, 2nd ed.; Elsevier: Amsterdam, 1984; pp 612.

Table 3. Estimated H_{ab} and α Values for Mixed-Valence States of Ferrocenyl-Containing Porphyrins Generated under Chemical- and Electrochemical Conditions

	ν_{max} (cm^{-1})	$\nu_{1/2}$ (cm^{-1})	ε_{IVCT}	r_{ab} (Å)[a]	H_{ab}	α
[*trans*-$H_2Fc_2Ph_2P$]$^{+b}$	12000	3200	6300	12.636	800	0.004
[*trans*-$H_2Fc_2Ph_2P$]$^{+c}$	11700	3400	16000	12.636	1300	0.012
[*trans*-$H_2Fc_2Ph_2P$]$^{+d}$	11700	2900	9300	12.636	910	0.006
[*cis*-$H_2Fc_2Ph_2P$]$^{+b}$	12000	2700	7700	9.810	1000	0.007
[*cis*-$H_2Fc_2Ph_2P$]$^{+c}$	11700	2500	15300	9.810	1400	0.014
[*cis*-$H_2Fc_2Ph_2P$]$^{+d}$	11000	4100	6100	9.810	1100	0.010
[*cis*-$H_2Fc_2Ph_2P$]$^{+b}$	12100	2700	7700	9.747	1100	0.008
[*cis*-$H_2Fc_2Ph_2P$]$^{+c}$	11700	2500	15300	9.747	1400	0.014
[*cis*-$H_2Fc_2Ph_2P$]$^{+d}$	11000	4100	6100	9.747	1100	0.010
$[H_2Fc_3PhP]^{+b}$	11300	2100	15000	9.793	1300	0.012
$[H_2Fc_3PhP]^{+c}$	11100	2100	39000	9.793	2000	0.032
$[H_2Fc_3PhP]^{+d}$	10700	1700	6000	9.793	700	0.004
$[H_2Fc_3PhP]^{+b}$	11300	2100	15000	12.189	1000	0.008
$[H_2Fc_3PhP]^{+c}$	11100	2100	39000	12.189	1600	0.021
$[H_2Fc_3PhP]^{+d}$	10700	1700	6000	12.189	600	0.003
$[H_2Fc_3PhP]^{2+b}$	8700	2300	8300	9.793	900	0.010
$[H_2Fc_3PhP]^{2+d}$	7800	2500	4900	9.793	600	0.007
$[H_2Fc_3PhP]^{2+b}$	8700	2300	8300	12.189	700	0.006
$[H_2Fc_3PhP]^{2+d}$	7800	2500	4900	12.189	500	0.004

[a] DFT calculated geometries. [b] Counter ion = $OSO_2CF_3^-$. [c] Counter ion = DDQ^-. [d] Counter ion = $TFAB^-$.

Conclusions

Four polyferrocenylpolyphenylporphyrin species were synthesized by a mixed condensation method and characterized by ^1H, ^{13}C, and variable temperature NMR; UV−vis−NIR; MCD; APCI; and HS-ESI mass spectrometry methods. Electrochemical studies revealed one ferrocenyl-based oxidation for H_2FcPh_3P, two ferrocenyl-based oxidations for *cis*- and *trans*-$H_2Fc_2Ph_2P$, and three ferrocenyl-based oxidations for H_2Fc_3PhP, demonstrating the electrochemical formation of several mixed-valence compounds. It should be noted that the $\Delta E_{1/2}$'s of the compounds studied are environmentally dependent, and the use of noncoordinating solvents and electrolytes enables observation of the naked redox processes. Mixed-valence species similar to those found in H_2TFcP were confirmed in *cis*- and *trans*-$H_2Fc_2Ph_2P$ and H_2Fc_3PhP by spectroelectrochemical and chemical oxidations (UV−vis−NIR) by the presence of NIR IVCT bands that were analyzed using the Hush method and found to be class II (Robin and Day) in character. The electronic structure calculations done at the density functional theory level found that the porphyrin ring was progressively distorted in a saddle conformation as ferrocenyl groups were added to the ring. The HOMO and lower-lying orbitals in H_2FcPh_3P, *trans*-$H_2Fc_2Ph_2P$, and H_2Fc_3PhP were mainly ferrocene-based orbitals, while the LUMOs and LUMO(+1)s were predominately porphyrin centered and near-degenerate. Despite the conformational flexibility of the ferrocenyl groups on the porphyrin core and metal−metal distances greater than 12 Å, mixed-valence species were formed electrochemically and chemically, most likely due to the porphyrin-Cp π system allowing the Fe centers a pathway to couple. The electrochemical and spectroscopic signatures of the polyferrocenylpolyphenyl porphyrins continue the trend set by H_2TFcP, adding further evidence supporting spin-localized, class II systems. The complete characterization of polyferrocenylpolyphenyl porphyrins demonstrated that these compounds, even with two ferrocenyl moieties, gave intervalence charge transfer bands, thus indicating their potential utility in electronic devices.

Supporting Information Available: ^1H, ESI, APCI, and HRMS spectra and frontier MOs of target compounds. DFT predicted geometries for ferrocenyl-containing porphyrins. Chemical and electrochemical reductions of [*cis*-$H_2Fc_2Ph_2P$]$^+$, [*trans*-$H_2Fc_2Ph_2P$]$^+$, $[H_2Fc_3PhP]^+$, and $[H_2Fc_3PhP]^{2+}$ into corresponding neutral complexes. Full citation for Gaussian 03. Molecular orbital and TDDFT compositions. CIF file for H_2TFcP structure. This material is available free of charge via the Internet at http://pubs.acs.org.

Acknowledgment. Generous support from NSF CHE-0809203, NSF CHE-0922366 (X-ray diffractometer), and Minnesota Supercomputing Institute to V.N.N. as well as University of Minnesota Duluth Undergraduate Research Opportunity Grants to R.G.H., J.R.S., and C.D.B. is greatly appreciated.